The Kidney Contains Ontogenetically Distinct Dendritic Cell and Macrophage Subtypes throughout Development That Differ in Their Inflammatory Properties

Natallia Salei,[1,2] Stephan Rambichler,[1,2] Johanna Salvermoser,[1,2] Nikos E. Papaioannou,[1,2] Ronja Schuchert,[3,4] Dalia Pakalniškytė,[1,2] Na Li,[5,6] Julian A. Marschner,[6] Julia Lichtnekert,[6] Christopher Stremmel,[3,4] Filippo M. Cernilogar,[7] Melanie Salvermoser,[1,2] Barbara Walzog,[1,2] Tobias Straub,[8] Gunnar Schotta,[7,9] Hans-Joachim Anders ⓘ ,[6] Christian Schulz,[3,4] and Barbara U. Schraml ⓘ [1,2]

Due to the number of contributing authors, the affiliations are listed at the end of this article.

ABSTRACT

Background Mononuclear phagocytes (MPs), including macrophages, monocytes, and dendritic cells (DCs), are phagocytic cells with important roles in immunity. The developmental origin of kidney DCs has been highly debated because of the large phenotypic overlap between macrophages and DCs in this tissue.

Methods We used fate mapping, RNA sequencing, flow cytometry, confocal microscopy, and histocytometry to assess the origin and phenotypic and functional properties of renal DCs in healthy kidney and of DCs after cisplatin and ischemia reperfusion–induced kidney injury.

Results Adult kidney contains at least four subsets of MPs with prominent *Clec9a*-expression history indicating a DC origin. We demonstrate that these populations are phenotypically, functionally, and transcriptionally distinct from each other. We also show these kidney MPs exhibit unique age-dependent developmental heterogeneity. Kidneys from newborn mice contain a prominent population of embryonic-derived MHCII^{neg}F4/80^{hi}CD11b^{low} macrophages that express T cell Ig and mucin domain containing 4 (TIM-4) and MER receptor tyrosine kinase (MERTK). These macrophages are replaced within a few weeks after birth by phenotypically similar cells that express MHCII but lack TIM-4 and MERTK. MHCII[+]F4/80^{hi} cells exhibit prominent *Clec9a*-expression history in adulthood but not early life, indicating additional age-dependent developmental heterogeneity. In AKI, MHCII[neg]F4/80^{hi} cells reappear in adult kidneys as a result of MHCII downregulation by resident MHCII[+]F4/80^{hi} cells, possibly in response to prostaglandin E2 (PGE2). RNA sequencing further suggests MHCII[+]F4/80^{hi} cells help coordinate the recruitment of inflammatory cells during renal injury.

Conclusions Distinct developmental programs contribute to renal DC and macrophage populations throughout life, which could have important implications for therapies targeting these cells.

Macrophages, monocytes, and dendritic cells (DCs) are important innate immune sentinels that also play crucial roles in organ homeostasis.[1–6] They are located in most tissues of the body and are collectively known as mononuclear phagocytes (MPs) because they were originally thought to share a common monocyte origin.[1,4,7] Through the use of improved fate-mapping models and single-cell technologies, numerous studies have

unequivocally established that macrophages, monocytes, and DCs constitute developmentally distinct cell lineages with unique functions in immunity.[1] It has also become increasingly clear that even at steady state, accurate and reliable distinction of monocyte, DC, and macrophage subsets based on surface markers is complex due to the existence of distinct age-dependent developmental programs that contribute to MP networks across tissues and because MPs exhibit a degree of tissue-specific adaptation.[1,6,8]

Macrophage poiesis begins before birth and, in mice, primitive macrophage progenitors appear in the yolk sac (YS) as early as embryonic day (E) 7.25.[8–10] From E8.25, in a second wave of macrophage poiesis, erythro-myeloid progenitors are generated in the YS that enter the embryo proper between E8.5 and E12.5, give rise to macrophages in various organs, and contribute to fetal liver hematopoiesis.[11–13] Embryonic-derived macrophages, arising from primitive YS progenitors or erythro-myeloid progenitors, can persist into adulthood due to self-renewal in brain, lung, or liver in steady-state conditions.[1,4,6,14] From E10.5, hematopoietic stem cells (HSCs) arise in the dorsal aorta and migrate to the liver to initiate fetal definitive hematopoiesis, which later shifts to the bone marrow.[6] With increasing age, HSC-derived monocytes can also differentiate into long-lived macrophages and, in some tissues such as heart or testes, these monocyte-derived cells coexist side by side with macrophages of embryonic origin.[15,16] In intestine and dermis, which are exposed to a specific microbial environment, monocyte-derived cells are thought to fully replace embryonic-derived macrophages over time,[6,17] although in the gastrointestinal tract some tissue-resident macrophages appear to self-maintain independently of monocytic input.[18,19] The signals that regulate the tissue-specific ontogenetic diversity of macrophages remain ill defined.

DCs and monocytes arise from definitive hematopoiesis and their differentiation is well understood in adult mice. Adult bone marrow contains a fraction of progenitor cells capable of generating monocytes, plasmacytoid DCs (pDCs), and conventional or classic DCs (cDCs) and has therefore been termed macrophage and DC progenitor.[20] This bone marrow fraction further gives rise to common monocyte progenitors and so called common DC progenitors (CDPs) that exclusively generate monocytes and cDCs/pDCs, respectively.[21,22] CDPs further differentiate into pre-cDCs, which terminally differentiate into the two main cDC1 and cDC2 subtypes in peripheral organs in response to environmental cues.[1,2,23] Within CDPs the expression of the C-type lectin receptor DNGR-1 (encoded by the *Clec9a* gene) distinguishes cells with exclusive cDC potential and DNGR-1 continues to be expressed on pre-cDCs.[24] Although the *Clec9a* promoter is active in cDC1s and pDCs, it is not active in progenitors for other lymphoid and myeloid lineages—including precursors for monocytes, granulocytes, or lymphoid cells—and therefore mice expressing CRE-recombinase (CRE) under the *Clec9a* promoter allow for faithful tracing of the cDC lineage in steady state as well as in inflammation.[24,25]

Significance Statement

The origin of kidney dendritic cells (DCs) has been highly debated because they share many phenotypic traits with macrophages in this tissue. Using fate mapping, the authors demonstrate that kidneys from adult mice contain four subsets of DCs unique age-dependent differences in DCs and macrophages. Renal embryonic-derived macrophages are replaced shortly after birth by phenotypically similar cells arising from hematopoiesis. In adults, these are generated from DC progenitors. In two models of renal injury, cells resembling embryonic-derived macrophages reappear in inflamed kidneys as a result from MHCII downregulation from renal dendritic cells. Understanding age-dependent developmental aspects in these cells of immune-modulatory and antigen-presenting function may help scientists develop therapies targeting them.

Using *Clec9a-Cre*–mediated fate mapping, we have demonstrated that the steady-state adult kidney, when compared with other organs, contains numerous cells with high expression of the putative monocyte/macrophage markers CD64 and F4/80 that show substantial *Clec9a*-expression history, indicative of a CDP origin.[24] Renal CD64^{+} cells can further be distinguished based on differential expression of F4/80 and CD11b into F4/80^{hi} and CD11b^{hi} cells,[24,26] thus phenotypically resembling embryonic-derived macrophages and monocyte-derived cells, respectively.[12,27,28] CD11b^{hi} cells arise from CDP in adoptive transfers,[24] require the DC growth factor FMS-like tyrosine kinase 3 ligand (FLT3L) for their development and phenotypically resemble cDC2 based on high expression of the signature cDC2 transcription factor IRF4 and low levels of IRF8.[26] It has therefore been suggested that renal CD11b^{hi} cells are cDC2s that express CD64.[26] However, whether renal cDC2s and CD11b^{hi} cells share the same transcriptional requirements and resemble each other in comparative gene expression analysis has not been investigated.

Renal F4/80^{hi} cells resemble DCs in their ability to activate naive T cells,[24] but these cells also exhibit prominent phenotypic overlap with embryonic-derived macrophages.[26,29–31] We and others were unable to confirm the CDP origin of renal F4/80^{hi} cells using adoptive transfers of CDPs or pre-cDCs.[24,32] However, bone marrow progenitors can contribute to renal F4/80^{hi} cells in lethally irradiated mice and after depletion of HSCs by conditional deletion of the HSC master regulator *Myb* in *Mx-1^{cre}Myb^{flox/flox}* chimeric mice.[12,24] Fate mapping of adult HSCs in *Flt3-Cre* mice further corroborates the HSC origin of this population in steady-state adult kidney because about 50% of renal F4/80^{hi} cells display FLT3 expression history.[12,16] In contrast to these findings, renal F4/80^{hi} cells exchange poorly between parabiotic partners, indicating HSC-independent maintenance, although a poor exchange of blood monocytes between partner mice, as well as low chimerism in kidney compared with other organs,[33–36] could have led to an underestimation of blood contribution to kidney-resident leukocyte populations. Fate mapping of YS progenitors in mice carrying a tamoxifen-inducible CRE driven by the *Csfr-1* promoter (*Csf1r^{Mer-iCre-Mer}*)

demonstrates a YS contribution to renal F4/80^{hi} cells in early life that disappears within a few weeks after birth.[11,12,16] Taken together, these data indicate an age-dependent ontogenetic diversity of renal F4/80^{hi} cells and highlight that the precise origins of this population throughout life remain controversial.

In this study, we revisit the origin of kidney DC and macrophage populations in mice throughout development. We demonstrate that adult kidney contains at least four transcriptionally and functionally distinct cell populations with prominent *Clec9a*-expression history, indicative of DC origin. Of these, renal F4/80^{hi} cells bear phenotypic and transcriptional similarities to embryonic-derived macrophages. However, using fate mapping, we demonstrate that embryonic-derived macrophages do not show *Clec9a*-expression history and do not persist in kidney into adulthood. Instead, we find that YS-derived macrophages, which lack MHC class 2 (MHCII) expression, dominate the kidney at birth but are lost within the first few weeks of life. Their loss coincides with the appearance of MHCII[+]F4/80^{hi} cells that arise from definitive hematopoiesis but lack *Clec9a*-expression history in early life. At a time when MHCII[neg] YS erythro-myeloid progenitor–derived macrophages and MHCII[+]F4/80^{hi} cells coexist, MHCII[neg]F4/80[hi] macrophages preferentially localize to the renal medulla; whereas MHCII[+]F4/80^{hi} cells spread throughout the medulla and cortex. During cisplatin and ischemia reperfusion–induced AKI, MHCII[neg]F4/80^{hi} cells reappear in adult kidneys. These cells do not arise from *de novo* cell differentiation but are the result of MHCII downregulation by tissue-resident MHCII[+]F4/80^{hi} cells. Taken together, our studies suggest that at least three distinct developmental programs contribute to the kidney MP compartment during development and reveal a previously unappreciated age-dependent ontogenetic heterogeneity of renal MPs.

METHODS

Mice

Clec9a-Cre,[24] *Rosa26[-lox-STOP-lox-EYFP]*,[37] *ROSA26[-lox-STOP-lox-tdtomato]*,[38] *Cx3cr-1-green fluorescent protein (GFP)*,[39] *c-Myb^{−/−}*,[40] *Csf1r[Mer-iCre-Mer]*,[41] *Mx-1[Cre]*,[42] *Myb[flox/flox]*,[43] and C57BL/6J mice were bred at the Biomedical Center or Walter Brendel Centre for Experimental Medicine (Ludwig Maximilian University of Munich, Martinsried, Germany) in specific pathogen-free conditions. For timed mating, mice of desired genotypes were mated overnight. Embryonic development was estimated considering the day of vaginal plug formation as E0.5. Mice at the age of 8–12 weeks were considered as adults. All animal procedures were performed in accordance with national and institutional guidelines for animal welfare and approved by the Regierung of Oberbayern (district government of Upper Bavaria).

Cell Isolation

Organs were isolated from mice after perfusion with cold PBS and cut into small pieces. Kidneys were digested in 2 ml of RPMI (Thermo Fisher Scientific) with 200 U/ml collagenase IV (Worthington) and 0.2 mg/ml DNAse I (Roche) for 1 hour at 37°C while shaking (120 rpm). After digestion, cells were passed through a 70-μm strainer and washed once with FACS buffer. Leukocytes were enriched using a 70%–37%–30% Percoll gradient by centrifugation (2000 rpm for 30 minutes at room temperature [RT]). Cells were collected at the 70%–37% interface. Percoll (100%) was prepared by adding nine parts of Percoll (GE Healthcare) to one part of 10× concentrated PBS. After Percoll enrichment, cells were washed once and resuspended in FACS buffer (PBS with 1% FBS, 2.5 mM EDTA [Invitrogen], 0.02% sodium azide [Sigma-Aldrich]) for analysis. For functional assays and sorting for RNA sequencing (RNA-seq), FACS buffer without sodium azide was used. Organs from mice up to 3 weeks old were collected without perfusion.

Spleen was digested in 1 ml of RPMI for 30 minutes as above. After digestion, cells were passed through a 70-μm strainer and washed once with FACS buffer. Erythrocytes were lysed with Red Blood Cell Lysing Buffer Hybri-Max (Sigma-Aldrich) for 2 minutes at RT, washed once, and resuspended in FACS buffer for further analysis.

Liver was digested in 2 ml PBS containing magnesium and calcium ions (Sigma-Aldrich) with 1 mg/ml collagenase IV, 60 U/ml DNAse I, 2.4 mg/ml Dispase II (Roche), and 3% FBS (Sigma-Aldrich) for 30 minutes at 37°C while shaking (120 rpm). After digestion, cells were passed through a 100-μm strainer, washed once with FACS buffer, and resuspended in FACS buffer for analysis.

Flow Cytometry

For surface staining, cells were incubated with 50 μl purified anti-mouse CD16/32/FcBlock for 10 minutes at 4°C. Additional antibodies were then added in FACS buffer to a final volume of 100 μl at 4°C for 20 minutes. After staining, cells were washed twice and resuspended in FACS buffer for analysis. Dead cells were identified with 4′,6-diamidino-2-phenylindole (DAPI; Sigma-Aldrich). For intracellular staining, cells were first stained with antibody against extracellular epitopes, and dead cells were identified with Fixable Viability Dye eFluor 780 (Thermo Fisher Scientific) or Zombie UV dye (Biolegend). Stained cells were fixed with 2% paraformaldehyde at RT for 15 minutes, and then washed with FACS buffer. Intranuclear staining was performed by using a Foxp3 Transcription Factor Staining Set (Thermo Fisher Scientific) according to the manufacturer's protocol. Intracellular staining for cytokine detection was performed by using the Intracellular Fixation and Permeabilization Buffer Set (Thermo Fisher Scientific) according to the manufacturer's protocol.

Flow cytometry was performed on an LSR Fortessa (BD Biosciences) with subsequent data analysis using FlowJo software (Tree Star). Cell sorting was performed on an Aria III Fusion (BD Biosciences). Cells were quantified by using CountBright Absolute Counting Beads (Thermo Fisher Scientific).

The following antibodies were purchased from Biolegend: anti–CD45.2-Alexa Fluor (AF) 700 (clone 104), anti–CD45.2-R-phycoerythrin-cyanine 7 (PECy7; clone 104), anti-MHCII I-A/I-E-AF700 (clone M5/114.15.2), anti-MHCII I-A/I-E-Allophycocyanin-cyanine 7 (APC-Cy7; clone M5/114.15.2), anti-MHCII I-A/I-E-Pacific Blue (PB; clone M5/114.15.2), anti–MHCII-Brilliant Violet (BV) 510 (clone M5/114.15.2), anti–CD11b-BV421 (clone M1/70), anti–CD11b-APC-Cy7 (clone M1/70), anti–CD11c-BV786 (clone N418), anti–CD11c-APC-Cy7 (clone N418), anti–CD3ε-PECy5 (clone 145–2C11), anti–CD19-BV650 (clone 6D5), anti–Ly6G-Peridinin-chlorophyll (PerCP)-Cy5.5, anti–CD205-PECy7 (clone NLDC-145), anti–F4/80-BV605 (clone BM8), anti–F4/80-BV786 (clone BM8), anti–F4/80-AF647 (clone BM8), anti–CD24-BV605 (clone M1/69), anti–XCR1-BV650 (clone ZET), anti–CD64-PE (clone ×54–5/7.1), anti–CD64-APC (clone X54-5/7.1), anti–CD64-biotin (clone X54-5/7.1), anti–IRF4-AF647 (clone IRF42EA), anti–TNFα-PECy7 (clone MP6-XT22), anti–IL-12/IL-23 p40-PE (clone C15.6), anti–Ly6C-BV605 (clone HK1.4), and anti–Ly6C-PB (clone HK1.4). Streptavidin-BV711 and streptavidin-PE was also purchased from Biolegend.

The following antibodies were purchased from BD Biosciences: anti–CD11b-Brilliant UltraViolet (BUV) 737 (clone M1/70), purified anti-CD16/32 (clone 2.4G2), and anti–ZBTB46-PE (clone U4-1374). Anti–MERTK-PerCPeFluor710 (PerCPeFluor710; clone DS5MMER) and anti–IRF8-PE (clone V3GYWCH) were purchased from Thermo Fisher Scientific. Anti–Mer-Biotin (clone unknown, catalog number BAF591) was purchased from R&D systems.

EdU Labeling

EdU (5-ethynyl-2′-deoxyuridine; Thermo Fisher Scientific) was dissolved in sterile infusion solution (Fresenius Kabi) and injected intraperitoneally (i.p.) at a dose of 0.1 mg/g body wt. Mice were euthanized 6 hours after injection. EdU was detected by using the Click-iT EdU Alexa Fluor 647 Flow Cytometry Assay Kit (Thermo Fisher Scientific) according to the manufacturer's protocol.

Pulse Labeling of YS-Derived Macrophages

For labeling of YS-derived macrophages, $Csf1r^{Mer-iCre-Mer}$ mice were crossed with heterozygous $Rosa26\text{-}^{lox\text{-}STOP\text{-}lox\text{-}EYFP}$ reporter mice. Pregnant females were injected at E8.5 with a single dose of 75 μg/g body wt of 4-hydroxytamoxifen (Sigma-Aldrich) supplemented with 37.5 μg/g body wt progesterone (Sigma-Aldrich). Kidneys and livers of F1 mice were analyzed at E18.5 and 2 weeks after birth by flow cytometry.

Conditional Deletion of Myb

$Mx\text{-}1^{Cre}Myb^{flox/flox}$ mice received four i.p. injections of polyinosinic-polycytidylic acid (polyI:C) every other day at a dose of 10 μg/g body wt.[44] Mice were then transplanted with 1×10^{7} CD45.1^{+} congenic wild-type bone marrow cells. At 3 and 9 months after bone marrow transplantation, mice were euthanized, and kidney and liver were analyzed by flow cytometry.

Transwell Chemotaxis Assay

A total of 0.5×10^{5} leukocytes from kidneys were added to the upper well of a transwell support (pore size of 5.0 μm; Corning) on a 24-well plate containing 100 ng/ml recombinant mouse CCL19 and CCL21 (Peprotech) in complete medium (RPMI supplemented with 10% FCS, penicillin/streptomycin, 1% nonessential amino acids, sodium pyruvate, L-glutamine, 0.05 mM β-mercaptoethanol). Cells were incubated at 37°C in humidified atmosphere containing 5% carbon dioxide. After 2 hours, cells were collected from the bottom well and analyzed by flow cytometry. The number of migrated cells per population was quantified by using CountBright Absolute Counting Beads (Thermo Fisher Scientific). The percentage of migrated cells per population was calculated by dividing the cell number from the bottom well to the input number of the respective population.

In Vitro Stimulation with Toll-Like Receptor Ligands

A total of 1×10^{5} kidney leukocytes were seeded in 200 μl complete medium (RPMI supplemented with 10% FCS, penicillin/streptomycin, 1% nonessential amino acids, sodium pyruvate, L-glutamine, 0.05 mM β-mercaptoethanol) and stimulated with resiquimod (R848; 2 μg/ml; Sigma-Aldrich), LPS (lipopolysaccharide, 100 ng/ml; Enzo), or zymosan (10 μg/ml; Sigma-Aldrich). After 2 hours, brefeldin A (5 μg/ml; Biolegend) was added and cells were incubated for an additional 4 hours before analysis by intracellular cytokine staining and flow cytometry.

Cisplatin-Induced AKI

AKI was induced in 10-week-old female $Clec9a^{cre/cre}Rosa^{YFP}$ mice by i.p. injection of cisplatin (15 mg/kg body wt). Sodium chloride was injected as a control for kidney damage. Blood, kidneys, and spleen were collected 72 hours after injection. Serum was isolated from blood for creatinine and BUN measurements using a Cobas Integra 400 Plus analyzer (Roche). Creatinine was detected using a cobas c pack CREP2 (Roche) and BUN was measured with a cobas c pack UREAL (Roche). Kidneys and spleen were processed for flow cytometry.

Unilateral Ischemia-Reperfusion Injury

Unilateral ischemia-reperfusion injury was induced in 10-week-old male $Clec9a^{cre/cre}Rosa^{YFP}$ mice as previously described.[45] Briefly, an anesthesia mixture containing medetomidine, midazolam, and fentanyl was applied before surgery. Online rectal temperature recording was then installed for every mouse. The left unilateral renal pedicle of each mouse was clamped for 25 minutes with a micro aneurysm clamp (Medicon) after a flank incision. Body temperature was continuously measured with a rectal probe and maintained at 36.5–38.5°C by placing the mice on a heating plate. After clamping, the kidney was placed back inside the abdomen. After clamp removal, the kidney was inspected for color change from pale (ischemia) to the original color before closing wounds with absorbable sutures for the peritoneal and

cutaneous layer (Ethicon). To maintain fluid balance, all mice were supplemented with 200 μl of saline. Three days after surgery, kidneys were isolated and analyzed as described above.

RNA Isolation and Library Construction

Total RNA was isolated using the column-based PicoPure RNA Isolation Kit (Thermo Fisher Scientific). RNA quality was assessed using a 2100 Bioanalyzer (Agilent) and samples with an RNA integrity number of more than eight were used for cDNA synthesis by using the ultra-low input RNA SMART-Seq v4 Kit (Clontech) according to the manufacturer's instructions. cDNA was transferred to AFA Fiber Pre-Slit Snap-Cap 6×16 mm microTUBEs (Covaris) and sheared by sonication using a Covaris S220 instrument. Sheared cDNA was cleaned using ethanol precipitation and sonication efficiency was determined using the Agilent 2100 Bioanalyzer. A maximum of 10 ng sheared cDNA was used to generate libraries for RNA-seq with the MicroPlex Library Preparation Kit v2 (Diagenode). The libraries were amplified until a DNA concentration >5 ng/μl was reached as determined by Qubit 2 DNA quantification (Thermo Fisher Scientific). Amplified libraries were cleaned using AMPure XP beads (Beckman Coulter) as described in the SMART-seq v4 Kit protocol, and the final concentration as well as the purity of the libraries were assessed using a 2100 Bioanalyzer. Sequencing was performed on an Illumina HiSeq1500 sequencer with 50-bp single-end reads and a sequencing depth of 20 million reads.

RNA-Seq Analysis

RNA-seq reads were mapped to the mouse genome (mm10) using STAR.[46] Expression of genes in transcripts per kilobase million was calculated with RSEM.[47] RNA-seq analysis was performed in R (version 3.4.3) with RStudio (version 1.1.414). DESeq2 (version 1.18.1) was used for differential gene expression analysis and principal component analysis (PCA). Genes with average gene counts of less than one were discarded and log$_2$ fold-change shrinkage was performed using the Apeglm package.[48] *iCre* and *Gapdh* DNA sequences were loaded in R using Biostrings (version 2.50.1) and manual alignment was performed with Shortread (version 1.40.0). Heatmaps were generated using pheatmap (version 1.0.10) and graphs were plotted with ggplot2 (version 2.2.1). Sequencing data have been deposited in the Gene Expression Omnibus under accession numbers GSE131751 and GSE135921.

Immunofluorescence Microscopy

Kidneys were fixed overnight at 4°C in paraformaldehyde, dehydrated in phosphate buffer containing 30% sucrose overnight at 4°C,[49] transferred to Tissue-Tek O.C.T. (Sakura), and frozen on dry ice. Frozen sections (10 μm thick) were cut on a cryostat at −20°C (CM3050S; Leica), rehydrated in PBS, and permeabilized with PBS with 0.2% Triton X-100 (Sigma-Aldrich) or acetone (Sigma-Aldrich). Afterward, the sections were circled with a PAP Pen (Kisker Biotech GmbH) and blocked for 1 hour at RT in the dark with blocking

buffer containing 10% goat serum in PBS. Antibodies were diluted in blocking buffer and sections were incubated for 2 hours at RT in the dark with the antibody mixture. Finally, stained sections were washed with PBS, mounted with ProLong Diamond Antifade Mountant (Thermo Fisher Scientific), cured at RT for 24 hours in the dark, and stored at 4°C until imaging. Confocal microscopy was performed at the Core Facility Bioimaging of the Biomedical Center with an upright Leica SP8X WLL microscope equipped with a 405 nm laser, WLL2 laser (470–670 nm), and acousto-optical beam splitter. Three-dimensional tile scans were acquired with a 20×0.75 objective and image voxel size was 180 nm in the *x/y* direction and 0.5–1.3 μm in the *z* direction. The following channel settings were used: DAPI/BV421 (excitation, 405 nm; emission, 415–470 nm), AF488 (500 nm; 510–542 nm), tdTomato (553 nm; 563–591 nm), AF594 (592 nm; 605–640 nm), and AF647 (646 nm; 656–718 nm). Recording was done sequentially to avoid bleed through. BV421, AF488, AF594, AF647, and tdTomato were recorded with hybrid photo detectors and DAPI with a conventional photomultiplier tube. Tile scans were merged in LAS X (version 3.4.1.17670; Leica) and deconvolved using Huygens Professional (version 17.10.0p2.64b; Scientific Volume Imaging). Deconvoluted z-stacks were imported in Fiji[50] to create maximum projections, adjust brightness/contrast, and to add scale bars.

The following antibodies were purchased from Biolegend: anti-MHCII I-A/I-E-BV421 (clone M5/114.15.2), anti–CD11b-AF647 (clone M1/70), anti–CD31-AF488 (clone MEC13.3), anti–F4/80-AF594 (clone BM8), and anti–F4/80-AF647 (clone BM8). Anti-CD64 (50086-R027, rabbit IgG) was purchased from Sino Biologic, cleaved caspase-3 (clone D3E9, rabbit IgG) was purchased from Cell Signaling Technologies, goat anti-rabbit IgG-AF555 (A21429) was purchased from Thermo Fisher, and goat anti-rabbit IgG-AF488 (111-545-144) secondary antibody was ordered from Jackson ImmunoResearch. For quantification of MHCII^{neg}F4/80^{hi} cells and MHCII$^+$F4/80^{hi} cells, 300×300 μm cutouts were randomly chosen from cortex and medulla of deconvoluted tile scans. F4/80^{neg} cells were excluded using the Interactive Watershed plugin on the thresholded F4/80 channel. F4/80$^+$ cells with high expression of CD11b were not counted.

Histo-Cytometry

Histo-cytometry was adapted from Li *et al.*[51] Deconvoluted z-stacks were opened in Fiji for further processing. The z-stack was split in its channels and each channel was thresholded with the Auto Threshold plugin and default settings. The thresholded channels were recombined to a stack and transformed to a red-green-blue image. Noise was removed with the Despeckle plugin and the image was blurred with a Gaussian Blur filter and a 2-pixel radius to improve segmentation. The resulting image was transformed to an 8-bit image and segmentation was performed with the Interactive Watershed plugin. Using the same plugin, the selections for all segmented cells were imported from LabelMap to ROIManager. Finally, the selections were applied to the original deconvoluted tile

scan to measure area, position, shape descriptors, and mean channel intensity of each segmented cell. Results were combined to comma-separated value files, which were then converted to a flow-cytometry standard file for gating analysis using FlowJo software.

Statistical Analysis

Statistical significance was calculated using the two-tailed t test in Prism 7 software (GraphPad). Multiple comparison was performed by using one-way ANOVA. A P value <0.05 was considered significant.

RESULTS

The Adult Kidney Contains Four Subsets of CDP-Derived Cells

To characterize MPs of CDP origin in kidneys using flow cytometry, CD45$^+$ kidney leukocytes from $Clec9a^{cre/cre}Rosa^{YFP}$ mice were gated and MHCII$^+$ cells were identified independently of CD11c expression levels, because adult kidney harbors CDP-derived leukocytes that express little or no CD11c.[24] Within the CD45$^+$MHCII$^+$ fraction, CD11c$^-$CD64$^-$ cells constitute B cells and CD11c$^+$CD64$^-$ cells comprise the two main XCR-1$^+$CD11b$^-$ cDC1 and XCR-1$^-$CD11b$^+$ cDC2 populations (Figure 1A, Supplemental Figure 1A). CD64$^+$ cells can further be split based on differential expression of F4/80 and CD11b into F4/80^{hi}CD11b^{low} and CD11b^{hi}F4/80^{low} cells (Figure 1A).[24] For simplicity, we refer to these populations as F4/80^{hi} and CD11b^{hi} cells, respectively. As previously demonstrated, cDC1s exhibit near complete labeling with yellow fluorescent protein (YFP) in $Clec9a^{cre/cre}Rosa^{YFP}$ mice, whereas labeling of cDC2s is lower (83%±4%; Figure 1B). Increased labeling of cDC1s is to be expected because cDC1s express DNGR-1 in their differentiated form and thus can become labeled with YFP as fully mature cells.[24] In cDC2s, which lack DNGR-1, YFP labeling is a true indicator of cell origin (Figure 1B), although labeling of cDC2s is incomplete because some $Clec9a$ positive DC precursors escape labeling in $Clec9a^{cre}$ mice.[24] F4/80^{hi} and CD11b^{hi} cells also lack DNGR-1 expression[24] and label with YFP at 62%±11% and 50%±5%, respectively, indicating a CDP contribution to these populations (Figure 1B). No YFP labeling was observed in other lymphoid or myeloid cell lineages in the kidney, including MHCII^{neg}CD11b$^+$ cells, which include monocytes and neutrophils (Figure 1B, Supplemental Figure 1A). *In vivo* pulse labeling of proliferating cells with the thymidine analog EdU revealed that renal cDC2s showed lower homeostatic turnover than cDC1s but were comparable to CD11b^{hi} cells (Supplemental Figure 1B). F4/80^{hi} cells showed little to no EdU incorporation, indicating a slow homeostatic turnover of this population in steady-state kidney (Supplemental Figure 1B).

Because F4/80^{hi} and CD11b^{hi} populations labeled with YFP to a lower extent than cDC2s, we wanted to address whether the YFP$^+$ and YFP$^-$ F4/80^{hi} and CD11b^{hi} populations exhibit ontogenetic heterogeneity. Therefore, we performed phenotypic

analysis of kidney leukocytes using macrophage and DC markers. We first generated triple transgenic mice by crossing $Clec9a$-Cre mice to $Rosa^{lox-stop-lox-tomato}$ ($Rosa^{Tom}$)[38] and $Cx3cr1$-Gfp transgenic mice.[39] In these mice, the expression of CX3CR1 can be assessed by GFP fluorescence and in cells of CDP origin, which are marked by tomato fluorescence. $Rosa^{Tom}$ mice are efficient fate-reporter mice due to a short distance between the loxP sites and a strong promoter driving tomato expression.[52] Accordingly, the penetrance of CRE-mediated DNA rearrangement was increased in $Clec9a^{+/cre}Rosa^{Tom}Cx3cr-1^{+/GFP}$ mice compared with our observations in $Clec9a^{cre}Rosa^{YFP}$ mice.[24] Near complete labeling of renal cDC2s (97%±1%) and increased labeling of CD11b^{hi} cells (80%±5%) and F4/80^{hi} cells (73%±4%) was observed in $Clec9a^{+/cre}Rosa^{Tom}$ animals heterozygous for Cre (Figure 1D, left panel). Importantly, tomato signal remained restricted to CDP-derived cells in $Clec9a^{+/cre}Rosa^{Tom}Cx3cr-1^{+/GFP}$ mice (Supplemental Figure 1C). We therefore concluded that heterozygous $Clec9a^{+/cre}Rosa^{Tom}$ mice are efficient reporters of CDP origin and can be used for fate-mapping experiments interchangeably with homozygous $Clec9a^{cre/cre}Rosa^{YFP}$ mice.

CX3CR-1 is highly expressed in macrophages of embryonic origin, some tissue macrophage populations such as microglia and cardiac macrophages, and to a lower extent on monocyte-derived cells and some cDCs.[53] As expected, renal cDC1s lacked CX3CR1 expression, whereas cDC2s expressed low to intermediate levels of CX3CR1 (Figure 1D, right panel, Supplemental Figure 1D). The highest CX3CR1-GFP levels were observed in F4/80^{hi} cells (Figure 1D, right panel, Supplemental Figure 1D), consistent with previous reports,[30,31] and GFP levels did not differ between tomato-labeled and unlabeled F4/80^{hi} cells (Figure 1D, right panel, Supplemental Figure 1D). Notably, F4/80^{hi} cells, independent of whether they were displaying $Clec9a$-expression history or not, lacked expression of MERTK and TIM-4 (Figure 1E, Supplemental Figure 1E), markers typically associated with embryonic-derived or self-maintaining macrophages.[16,18,54,55] F4/80^{hi} cells also expressed low levels of the cDC-specifying transcription factors IRF4, IRF8, and ZBTB46 (Figure 1F, Supplemental Figure 1F). As reported, CD11b^{hi} cells principally resembled cDC2s based on high levels of IRF4 and ZBTB46, and concomitant low levels of IRF8 expression[26] (Figure 1F, Supplemental Figure 1F), but showed higher CX3CR1 and F4/80 expression than cDC2s (Figure 1, D and F, Supplemental Figure 1, D and F). Phenotypic analysis did not show obvious differences between CD11b^{hi} cells displaying $Clec9a$-expression history or not (Figure 1, D and F). Thus, F4/80^{hi} and CD11b^{hi} populations differ from each other and cDC1/2s in terms of marker expression, although no obvious phenotypic differences exist between the YFP$^+$ and YFP$^-$ fractions of these populations.

Renal CD11b^{hi} and F4/80^{hi} Cells Are Transcriptionally Distinct from cDC1 and cDC2

To further reveal differences between phenotypically similar cells displaying $Clec9a$-expression history or not, we performed transcriptome profiling by mRNA sequencing.
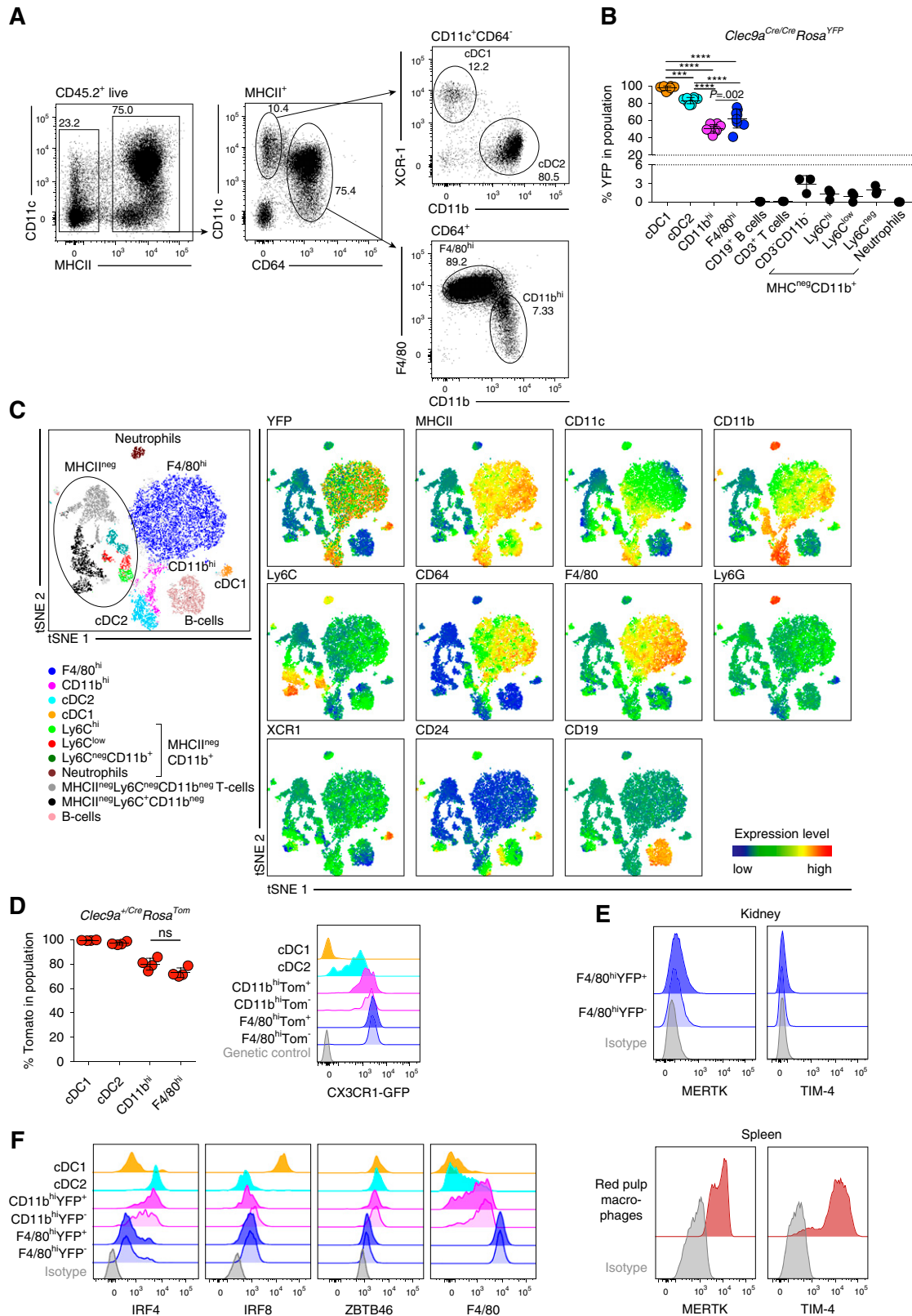
Figure 1. The adult kidney contains four phenotypically distinct subsets of MPs with *Clec9a*-expression history. (A–C) Kidney leukocytes from 10- to 12-week-old *Clec9a^cre/cre^Rosa^YFP^* mice were analyzed by flow cytometry. (A) Live CD45.2^+ MHCII^+ cells were gated as indicated and subdivided into CD11c^+CD64^− and CD64^+ cells. CD11c^+CD64^− cells were further analyzed for XCR-1 and CD11b expression to identify cDC1s and cDC2s, respectively. CD64^+ cells were further divided into F4/80^hi and CD11b^hi cells. (B) The

We sort purified the YFP$^+$ and YFP$^-$ fractions of F4/80^{hi} and CD11b^{hi} cells from kidneys of *Clec9a$^{cre/cre}$Rosa^{YFP}* mice and compared their gene expression profiles to those of cDC1s and cDC2s sorted as YFP$^+$ cells from the same organ (for gating strategy and sort purity see Supplemental Figure 2, A and B). As reference populations, splenic YFP$^+$ cDC1s, YFP$^+$ cDC2s, and red pulp macrophages (RPMs) were sorted. In PCA, reference cDC1s and cDC2s segregated from splenic RPMs on principal component 1 (PC1), revealing transcriptional differences between cDCs and macrophages (Figure 2A). PC2 identified tissue-specific differences in gene expression and uniformly separated populations sorted from spleen and kidney (Figure 2A). As expected, cDC1s and cDC2s from different organs clustered in close proximity on PC1 (Figure 2A). Notably, CD11b^{hi} cells segregated away from cDC1s and cDC2s in PCA (Figure 2A), indicating that they are transcriptionally distinct, although they more closely resembled cDC2 than cDC1. To our surprise, YFP$^+$ and YFP$^-$ CD11b^{hi} cells clustered together in PCA (Figure 2A) and showed few transcriptional differences in pairwise comparison (adjusted $P<0.05$, log$_2$ fold change$>$4; Figure 2C), demonstrating a strong transcriptional overlap. A strong resemblance was also observed between YFP$^+$ and YFP$^-$ F4/80^{hi} cells in PCA and pairwise comparison, and these populations unexpectedly clustered away from the other renal populations but close to RPM in PC1 (Figure 2, A and B). Because the *Clec9a*-expression history indicates a common origin of F4/80^{hi} cells with cDCs,[24] we would have expected a closer resemblance of F4/80^{hi} cells to cDCs, particularly in the YFP$^+$ fraction. Importantly, we detected no *Cre* expression in cDC2s, CD11b^{hi} cells, and F4/80^{hi} cells; whereas cDC1s showed strong expression of *Cre*, as expected (Supplemental Figure 2C). These data corroborate that these populations lack *Clec9a* promoter activity and therefore the YFP label must result from *Clec9a* expression at an earlier time.[24]

Because RNA-seq analysis did not reveal differences between YFP$^+$ and YFP$^-$ populations, we focused exclusively on CD11b^{hi} and F4/80^{hi} samples sorted as YFP$^+$ cells for further analyses. Using unsupervised, hierarchical k-means clustering of genes differentially expressed between renal cDC1s, cDC2s, CD11b^{hi} cells, and F4/80^{hi} cells, we defined 15 clusters of genes with distinct expression characteristics (Figure 2D). Of these, several clusters (II, VI, and XII) distinguished F4/80^{hi} cells and revealed lower expression of typical DC-associated genes, such as *Zbtb46*, *Flt3*, *Bcl11a*, and *Ccr7*, in F4/80^{hi} cells compared

with the other renal populations (Figure 1F, Supplemental Table 1).[26] Clusters XIII and XV contained genes with higher expression in F4/80^{hi} and CD11b^{hi} cells compared with cDC2s and cDC1s and included *FcgR1* (CD64), *Emr1* (F4/80), and *Cx3cr1* (Supplemental Table 1). Pairwise comparison of cDC2s and CD11b^{hi} cells identified 38 genes with a log$_2$ fold change greater than four (adjusted $P<0.05$; Figure 2E) and 180 genes with a log$_2$ fold change greater than two. Differentially expressed genes included several genes involved in pathogen defense such as *Tlr7*, *Tlr8*, and the complement receptor *C3ar1* (Figure 2E, Supplemental Table 2). Pairwise comparison of CD11b^{hi} cells with F4/80^{hi} cells revealed 362 genes with a log$_2$ fold change greater than four (adjusted $P<0.05$; Figure 2F, Supplemental Table 3). Higher expression of *Zbtb46*, *Flt3*, *Bcl11a*, and *Blhe40* in CD11b^{hi} cells confirmed a more classic cDC transcriptional signature in this population than in F4/80^{hi} cells (Figure 2F, Supplemental Table 3). In contrast, F4/80^{hi} cells had higher expression of several macrophage-associated genes such as *Slco2b1*, *VCam1*, and *Tmem119* (Figure 2F, Supplemental Table 3). Taken together, these analyses demonstrate that CD11b^{hi} and F4/80^{hi} cells are transcriptionally distinct from cDC1/2s, although it is noteworthy that CD11b^{hi} cells were more similar to cDC2s than cDC1s and F4/80^{hi} cells.

In response to TLR ligands, cDC1s were the most potent source of interleukin (IL)-12, because we detected high amounts of preformed IL-12 in this population even without prior stimulation (Figure 2, G–I, gating strategy in Supplemental Figure 3A). cDC1s were also the strongest producers of IL-12 in response to LPS and zymosan stimulation, although they did not respond to resiquimod (R848) stimulation with production of TNF or IL-12 (Figure 2, G–I). F4/80^{hi} cells were the most potent producers of TNF in response to R848, LPS, and zymosan (Figure 2, G–I) but they were poor producers of IL-12 under the tested conditions (Figure 2, G–I). cDC2s and CD11b^{hi} cells did not produce TNF in response to R848 (Figure 2G). Notably, more CD11b^{hi} cells than cDC2s produced IL-12 in response to R848 (Figure 2G), in line with higher TLR8 expression in these cells compared with cDC2s (Supplemental Figure 3B). In contrast, more cDC2s produced IL-12 in response to zymosan than CD11b^{hi} cells (Figure 2G), despite comparable expression of TLR2 and lower expression of Dectin1 (Supplemental Figure 3B). In this analysis we found a similar response between the YFP$^+$ and YFP$^-$ fractions

percentage of YFP$^+$ cells in the indicated populations (see also Supplemental Figure 1A) is shown. (C) Representative t-distributed stochastic neighbor embedding (tSNE) of kidney leukocytes. Cells were clustered independently of their YFP labeling and manually gated populations were overlaid on the tSNE plot in the indicated colors. Blue-to-red gradient indicates increasing intensity of marker expression. (D) Left panel shows the percentage of tomato$^+$ cells in each population; right panel, CX3CR-1-GFP expression in cDC1s, cDC2s, as well as F4/80^{hi} and CD11b^{hi} cells, further divided into tomato$^+$ and tomato$^-$ cells. Gray traces represent GFP fluorescence in control mice lacking the CX3CR-1-GFP allele. (E) Renal YFP$^+$ and YFP$^-$ F4/80^{hi} cells were analyzed for MERTK and TIM-4 expression by flow cytometry. Expression of these markers on splenic RPMs is shown as positive control. (F) Renal cDC1s, cDC2s, YFP$^+$ and YFP$^-$ F4/80^{hi} cells, as well as YFP$^+$ and YFP$^-$ CD11b^{hi} cells from *Clec9a$^{cre/cre}$Rosa^{YFP}* mice were analyzed for IRF4, IRF8, ZBTB46, and F4/80 expression. Gray traces represent staining with isotype-matched control antibodies. (B–D) Each dot represents one mouse, horizontal bars represent mean, error bars represent SD. ***$P<0.001$, ****$P<0.0001$.
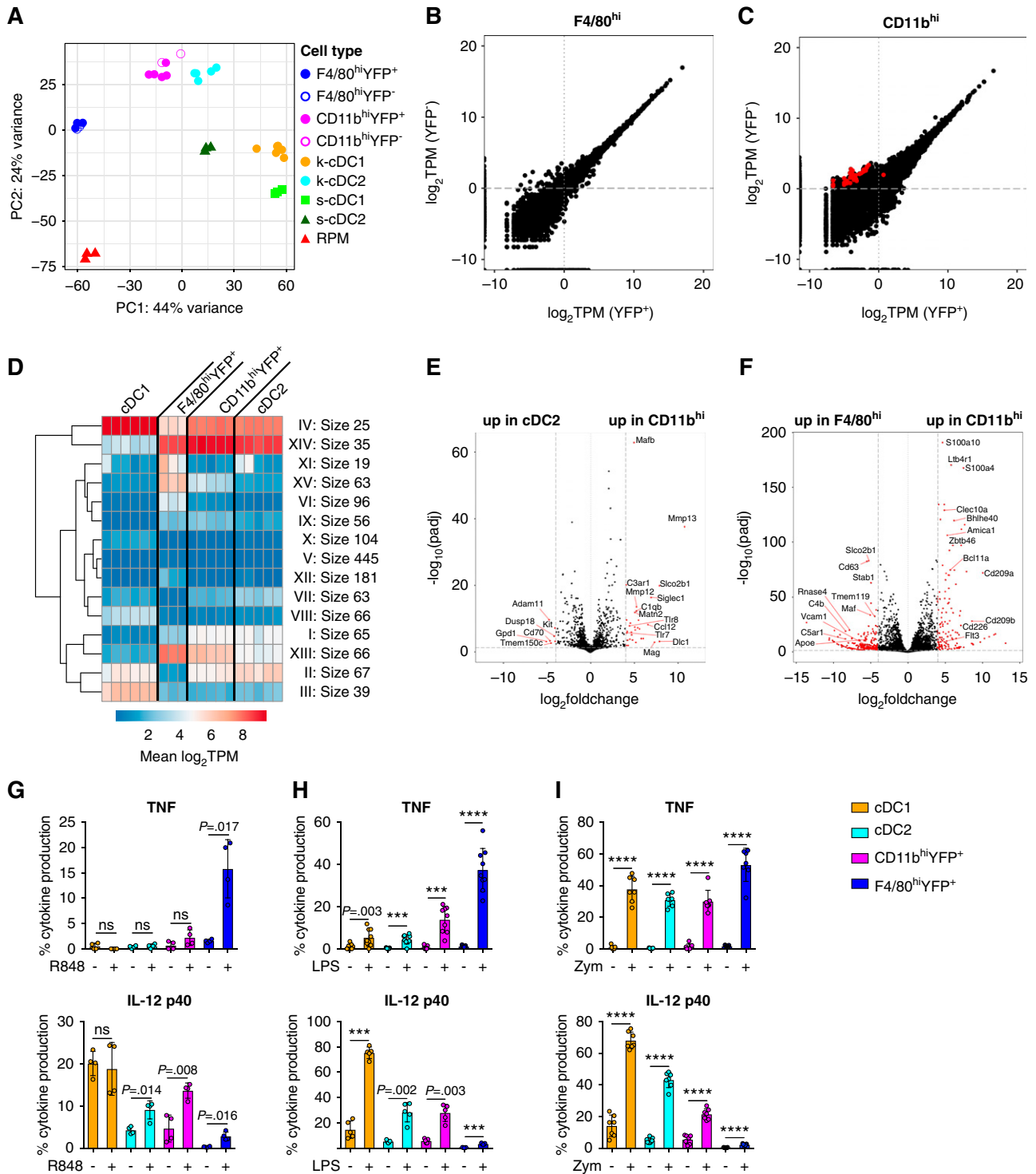
Figure 2. Renal F4/80^{hi} are transcriptionally distinct from cDC1s, cDC2s, and CD11b^{hi} cells. (A–F) YFP^{+} and YFP^{−} fractions of F4/80^{hi} and CD11b^{hi} cells as well as YFP^{+} cDC1s and YFP^{+} cDC2s were sorted from kidneys of adult *Clec9a*[cre/cre]*Rosa*[YFP] mice. Splenic YFP^{+} cDC1s, YFP[+] cDC2s, and RPMs were isolated as reference populations from the same mice. Sorted populations were subjected to mRNA-sequencing analysis. (A) PCA of the top 500 genes as defined by the highest variance across all samples. Each dot of the same color represents a biologic replicate. (B and C) Comparison of gene expression in (B) YFP^{+} and YFP^{−} F4/80^{hi} cells and (C) YFP^{+} and YFP^{−} CD11b^{hi} cells displayed as transcripts per kilobase million (TPM) reads. Red circles indicate genes with a log₂ fold change greater than four between samples and an adjusted *P* (padj)<0.05. (D) k-means clustering of differentially expressed genes (log₂ fold change>4; adjusted *P*<0.05) between renal cDC1s, cDC2s, YFP^{+} CD11b^{hi} cells, and YFP^{+} F4/80^{hi} cells. (E and F) Pairwise comparison

of F4/80^{hi} and CD11b^{hi} cells, respectively, although it is noteworthy that YFP^{−} F4/80^{hi} cells showed slightly reduced TNF production to LPS and zymosan compared with their YFP[+] counterparts (Supplemental Figure 3, C–E). CCR7 mediates migration of cDCs to lymph nodes and showed a relative paucity in expression in F4/80^{hi} and CD11b^{hi} cells when compared with cDC1s and cDC2s (Supplemental Table 1). Accordingly, cDC1s and cDC2s isolated from the steady-state kidney migrated toward the CCR7 ligands CCL19/21 in *in vitro* transwell chemotaxis assays (Supplemental Figure 3F). F4/80^{hi} and CD11b^{hi} cells failed to migrate toward CCL19/21 in the same assay (Supplemental Figure 3F). Taken together, these analyses show that cDC1s, cDC2s, CD11b^{hi} cells, and F4/80^{hi} cells are transcriptionally distinct populations of renal MPs that display the distinct ability to respond to pathogenic stimuli.

Renal Embryonic–Derived Macrophages Do Not Show *Clec9a*-Expression History

Considering that, despite exhibiting *Clec9a*-expression history, renal F4/80^{hi} cells resembled macrophages in terms of phenotype (Figure 1) and gene expression (Figure 2A), we wanted to exclude the possibility that renal YS-derived macrophages aberrantly label in *Clec9a[cre]* mice. We therefore isolated kidneys from *Clec9a[cre/cre]Rosa[YFP]* mice on E15, when macrophages with a F4/80[hi] phenotype predominantly arise from YS progenitors.[11–13,56,57] As expected, E15 kidneys from *Clec9a[cre/cre]Rosa[YFP]* mice contained F4/80^{hi} and CD11b^{hi} cells, which represent YS-derived macrophages and *Myb*-dependent HSC-derived cells, respectively.[12] Importantly, F4/80^{hi} cells did not show any YFP labeling in *Clec9a[cre/cre]Rosa[YFP]* mice (Figure 3A), whereas YFP^{+} cells could be found within the *Myb*-dependent CD11b^{hi} fraction of E15 kidneys,[12] indicating the *Clec9a* promoter is active at this stage of development (Figure 3A). These YFP^{+} cells uniformly expressed MHCII and CD11c, consistent with them being cDCs (Figure 3A and data not shown). Taken together, these data strongly support the notion that embryo-derived macrophages do not label with YFP in *Clec9a[cre/cre]Rosa[YFP]* mice.

To confirm this, we performed microscopic analysis of kidney sections from *Clec9a[cre/cre]Rosa[Tom]* mice 2 days after birth (postnatal day 2 [PND2]; Figure 3B). As expected, we found F4/80-expressing cells in newborn kidney that were spread throughout the medulla and cortex (Figure 3B), whereas tomato-positive cells were fewer in number and mostly lacked F4/80 expression (Figure 3B, white arrows). This was in striking contrast to kidney sections from adult *Clec9a[+/cre]Rosa[Tom]* mice, where tomato-positive cells costained with F4/80 showed dendritic shape and spread throughout the

entire kidney interstitium, as expected (Figure 3C).[24] Notably, in adult kidneys, a fraction of Tomato[+] F4/80^{hi} cells formed a discrete population around glomeruli (Figure 3C), which may indicate a role for these cells in monitoring the transendothelial transport of proteins and particles.[33] Taken together, these data demonstrate that the failure to detect *Clec9a*-expression history in renal F4/80[hi] YS-derived macrophages at E15 by flow cytometry was not due to an inability to isolate these cells from tissues. These data unequivocally establish that embryonic-derived macrophages are not aberrantly labeled in *Clec9a-Cre* mice, although we cannot formally exclude at this point that a persistent population of embryonic-derived macrophages acquires *Clec9a* expression and consequently YFP/tomato labeling in later life.

Dynamic Age-Dependent Changes in the Renal MP Network

We next asked when YFP^{+}F4/80^{hi} cells arise in kidneys of *Clec9a[cre/cre]Rosa[YFP]* mice (Figure 4, A and B). CD45^{+}MHCII^{+} cells could be identified as early as PND2 in the kidney, but their relative frequency was low compared with adult kidney (Figure 4, A and B). CD45^{+}MHCII^{+} cells divided into the expected CD64^{+} and CD64^{−} fractions on PND2 (Figure 4, A and B). MHCII^{+}CD64^{−} cells encompassed XCR-1^{+} cDC1s and CD11b^{+} cDC2s at all ages examined, as expected (not shown). Surprisingly, MHCII^{+}CD64^{+} kidney leukocytes uniformly displayed a CD11b^{hi} surface phenotype on PND2 (Figure 4A). The MHCII^{+}CD64^{+} F4/80^{hi} subset was observed 2 weeks after birth and, by 4 weeks of age, had become the dominant population of MHCII^{+}CD64^{+} cells (Figure 4A). Notably, F4/80^{hi} cells were present in kidneys of *Clec9a[cre/cre]Rosa[YFP]* mice on PND2 but they lacked MHCII expression (Figure 4, A and B). In newborn kidney, these MHCII[neg]F4/80^{hi} cells were more abundant in frequency and number than the other MP subtypes analyzed, but this population showed an age-dependent decrease and became a minority population of kidney leukocytes by 4 weeks of age and was not found in adult kidneys (Figure 4, A and B).

We next analyzed YFP expression in each of these populations in *Clec9a[cre/cre]Rosa[YFP]* mice over time. MHCII^{+}CD64^{−} cDCs, which encompass both cDC1 and cDC2, served as our reference population and, expectedly, showed near complete YFP labeling (93%±3%) in *Clec9a[cre/cre]Rosa[YFP]* mice as early as PND2 (Figure 4C). MHCII[neg]F4/80^{hi} cells did not label with YFP in *Clec9a[cre/cre]Rosa[YFP]* mice at all ages examined (Figure 4C). To our surprise and in contrast to our findings in adult mice, MHCII^{+} F4/80^{hi} and CD11b^{hi} cells showed a paucity in YFP labeling in early life when compared with their

---

of (E) cDC2s with YFP^{+} CD11b^{hi} cells or (F) YFP^{+} F4/80^{hi} with YFP^{+} CD11b^{hi} cells was performed on RNA-seq data using the DEseq2 plugin in R. Red circles indicate genes with a log$_2$ fold change greater than four between samples and an adjusted *P* value <0.05. (G–I) Renal leukocytes from adult *Clec9a[cre/cre]Rosa[YFP]* mice were isolated and stimulated *in vitro* with (G) R848, (H) LPS, or (I) zymosan (Zym) for 6 hours. Intracellular levels of TNF and IL-12 p40 were analyzed by flow cytometry. Each dot represents one mouse, error bars represent SD. ***P<0.001, ****P<0.0001.
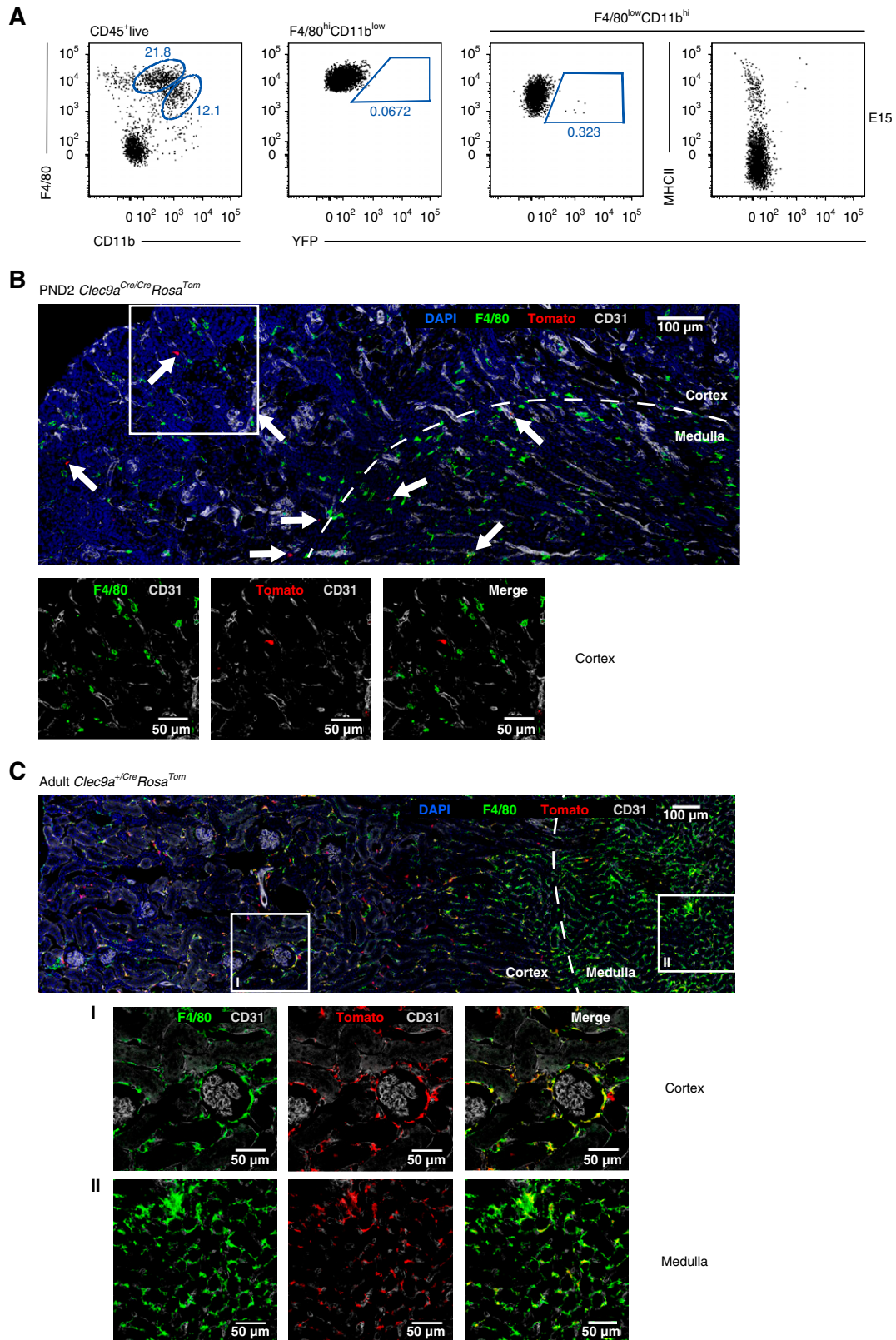
Figure 3. Embryonic macrophages do not show *Clec9a-Cre* expression history. (A) Kidneys from *Clec9a^{cre/cre}Rosa^{YFP}* mice were isolated at E15 and analyzed for F4/80 and CD11b expression by flow cytometry to identify F4/80^{hi} YS-derived macrophages and CD11b^{hi}F4/80^{low} cells. Populations were further analyzed for YFP and MHCII expression. (B and C) Immunofluorescence staining of kidneys from *Clec9a^{cre}Rosa^{Tom}* mice (B) at PND2 and (C) at 10 weeks of age. Kidney sections were stained for the following markers:

adult counterparts (Figure 4C). The lack of YFP labeling was especially pronounced in F4/80^{hi} cells, which acquired most of their YFP label after 4 weeks of age (Figure 4C). These data demonstrate that F4/80^{hi} cells do not arise from *Clec9a*-expressing cDC progenitors in early life. Importantly, the temporal differences in population expansion between MHCII^{neg}F4/80^{hi} cells and MHCII^{+}F4/80^{hi} cells in early life suggest a different ontogeny of these cells.

Renal MHCII^{neg}F4/80^{hi} Cells but Not F4/80^{hi} Cells Expressing MHCII Are Derived From Erythro-Myeloid Progenitors

Because the age-dependent loss of MHCII^{neg}F4/80^{hi} cells correlated with an increase in F4/80^{hi} cells (Figure 4B), we hypothesized that MHCII^{neg}F4/80^{hi} cells may represent YS-derived macrophages, which are described to lack MHCII in some tissues.[15,16,55] The transcription factor MYB is dispensable for YS myelopoiesis but it is required for the development of definitive HSCs and late erythro-myeloid progenitors arising from hemogenic endothelium, which generate macrophages via fetal liver monocytic intermediates.[11,40] MHCII^{neg}F4/80^{hi} cells developed normally in kidneys from *Myb*-deficient embryos at E16.5, confirming these cells arise independently of definitive hematopoiesis or *Myb*-dependent late erythro-myeloid progenitors (Figure 5A). In contrast, MHCII^{+} kidney leukocytes were strongly decreased in the absence of MYB (Figure 5A). Because F4/80^{hi} cells expressing MHCII are first established after birth (Figure 4, A and B), their MYB dependence cannot be analyzed in full knock-out mice, which are embryonically lethal. We therefore induced conditional deletion of the *Myb* gene in adult mice. To this end, CD45.2^{+}*Mx-1*^{Cre}*Myb*$^{flox/flox}$ mice were treated with polyI:C, which leads to a rapid loss of HSCs and their progeny that can be rescued without further preconditioning by transfer of congenic CD45.1^{+} bone marrow.[12,44] Three months after bone marrow rescue, chimeras were analyzed for bone marrow contribution to kidney MP subsets (Figure 5B). As expected, because of their HSC origin, cDCs were completely donor derived (Figure 5B). Similarly, CD11b^{hi} cells showed full donor origin, demonstrating they are HSC derived (Figure 5B). MHCII^{+}F4/80^{hi} cells were also strongly donor derived (53%±7%), although a considerable proportion of these cells remained of host origin 3 months after bone marrow rescue (Figure 5B). Notably, the replacement of F4/80^{hi} cells increased with time and, 9 months after bone marrow rescue, 74%±7% of cells had turned over (Supplemental Figure 4A). These data indicate that the incomplete donor chimerism is likely related to the relative longevity and low homeostatic turnover of this population in adult kidneys (Supplemental

Figure 1B). Thus, although F4/80^{hi} cells are not fully replaced by HSCs in the time frame analyzed, HSCs contribute to the maintenance of MHCII^{+}F4/80^{hi} cells in steady-state adult kidney.

To address whether YS-derived progenitors contribute to F4/80^{hi} cells, we took advantage of an established genetic model to fate map these cells in *Csf1r*$^{Mer-iCre-Mer}$ mice crossed to *Rosa*^{YFP} mice.[11,12,16] We treated pregnant dams at E8.5 with a single injection of 4-hydroxytamoxifen[12] and then analyzed the kidneys from offspring mice at E18.5 and 2 weeks after birth by flow cytometry (Figure 5C). Liver Kupffer cells, which derive in large proportions from YS erythro-myeloid progenitors[11,12] readily labeled with YFP at both ages examined (Figure 5C). On E18.5, renal MHCII^{neg}F4/80^{hi} cells also labeled with YFP, albeit at lower frequency than liver Kupffer cells and consistent with previous publications.[11–13] In contrast, CD64^{-} cDCs and CD11b^{hi} cells did not show YFP expression, as expected because of their HSC origin (Figure 5C). Importantly, 2 weeks after birth, when both MHCII-expressing and -nonexpressing F4/80^{hi} cells are present in kidneys, YFP signal was found exclusively on MHCII^{neg}F4/80^{hi} but not on MHCII^{+}F4/80^{hi}cells (Figure 5C), supporting that MHCII^{neg}F4/80^{hi} cells but not MHCII^{+}F4/80^{hi} cells arise from YS erythro-myeloid progenitors. Consistently, MHCII^{neg}F4/80^{hi} cells expressed higher levels of MERTK and TIM-4 than MHCII^{+}F4/80^{hi} cells, although expression levels of CX3CR1, F4/80, CD11c, and CD64 were similar (Figure 5D, Supplemental Figure 4B).

Because F4/80^{hi} cells were the most potent producers of TNF in response to several TLR ligands in adults (Figure 2, G–I), we analyzed TNF production of F4/80^{hi} cells and MHCII^{neg}F4/80^{hi} cells from 2- to 3-week-old mice in response to LPS, R848, and zymosan. Interestingly, neither MHCII^{+}F4/80^{hi} nor MHCII^{neg}F4/80^{hi} cells from 2-week-old mice produced TNF in response to R848 stimulation (Figure 5E), which is in contrast to F4/80^{hi} cells from adults (Figure 2G), although these cells express similar levels of TLR7/8 message (data not shown). MHCII^{+}F4/80^{hi} and MHCII^{neg}F4/80^{hi} cells from 2-week-old mice responded similarly to LPS and zymosan in terms of TNF production (Figure 5E), but again fewer cells produced TNF in response to these stimuli when compared with F4/80^{hi} cells from adult mice (Figures 2, H and I and 5E). We stained kidney sections from 2-week-old *Clec9a*^{Cre}*Rosa*^{Tom} mice with F4/80, CD11b, MHCII, and CD64 for microscopy (Figure 5F) and used histo-cytometry[51,58] to identify MHCII^{+}F4/80^{hi} and MHCII^{neg}F4/80^{hi} cells and distinguish them from CD11b^{hi} cells and cDC2s (Supplemental Figure 4, C and D). Notably, we found a strong bias for MHCII^{neg}F4/80^{hi} cells to localize in the renal medulla, whereas MHCII^{+}F4/80^{hi}

tomato (red), F4/80 (green), CD31 (gray), and DAPI (blue). Deconvoluted confocal tile scans were generated. (B) Arrows indicate tomato^{+} cells. Scale bar, 100 μm. Square marks the inset that is magnified below the tile scan to indicate absence of F4/80 signal on tomato^{+} cells. (C) Squares mark magnified areas of (I) the cortex or (II) the medulla that are shown below the tile scan image (scale bar, 50 μm) to indicate colocalization of F4/80 and tomato signal.
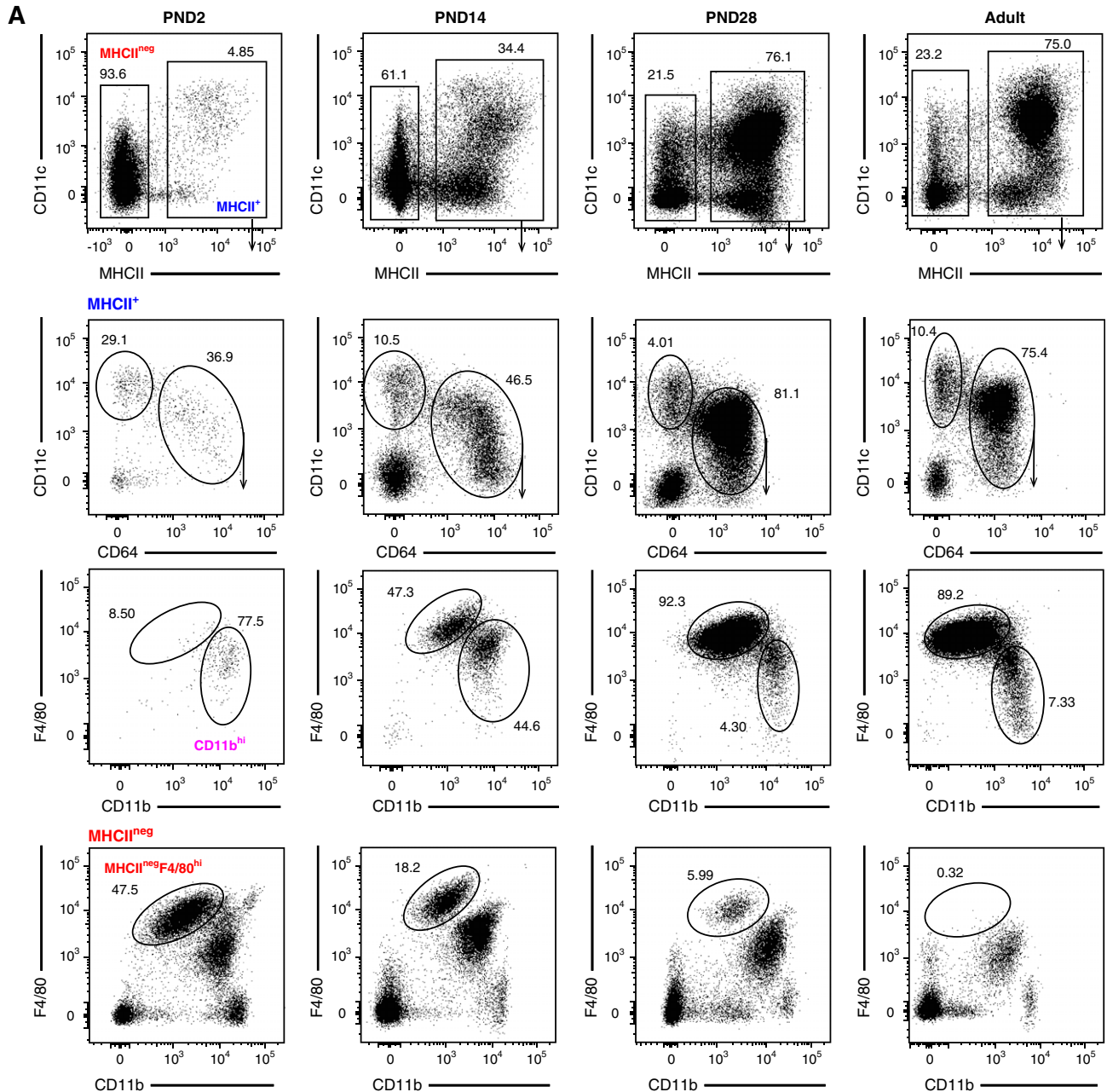
Figure 4. Renal MP populations exhibit dynamic age-dependent changes. (A–C) Kidneys isolated from *Clec9a^cre/cre Rosa^YFP* mice on PND2, PND14, PND28, and 10–12 weeks after birth were analyzed by flow cytometry. (A) Cells were first gated on live CD45.2$^+$ cells and further subdivided into MHCII^{neg} and MHCII$^+$ cells (top row). MHCII$^+$ cells were further analyzed for CD11c and CD64 expression (second row). MHCII$^+$CD64$^+$ cells (third row) and MHCII^{neg} cells (bottom row) were further analyzed for CD11b and F4/80 expression. (B) Frequency and total number of kidney CD64$^-$ cDCs, CD11b^{hi}, F4/80^{hi} and MHCII^{neg}F4/80^{hi} cells at the indicated ages are shown. (C) Percentage of YFP$^+$ cells in each population from *Clec9a^cre/cre Rosa^YFP* mice at the indicated ages. Each dot represents one mouse, horizontal lines indicate mean, error bars represent SD. ***$P<0.001$, ****$P<0.0001$, only statistically significant differences are marked.

cells spread more evenly across the kidney cortex and medulla (Figure 5G). Thus, early life MHCII^{neg}F4/80^{hi} cells represent YS erythro-myeloid progenitor–derived macrophages that are replaced over time with MHCII$^+$F4/80^{hi} cells arising in a *Myb*-dependent manner.

Renal F4/80^{hi} Cells from Adult Mice Downregulate MHCII Expression in Response to Renal Inflammation

To investigate DC dynamics after kidney injury, we injected *Clec9a^cre/cre Rosa^YFP* mice with cisplatin to induce AKI[59] and analyzed renal leukocyte populations for YFP expression 3 days
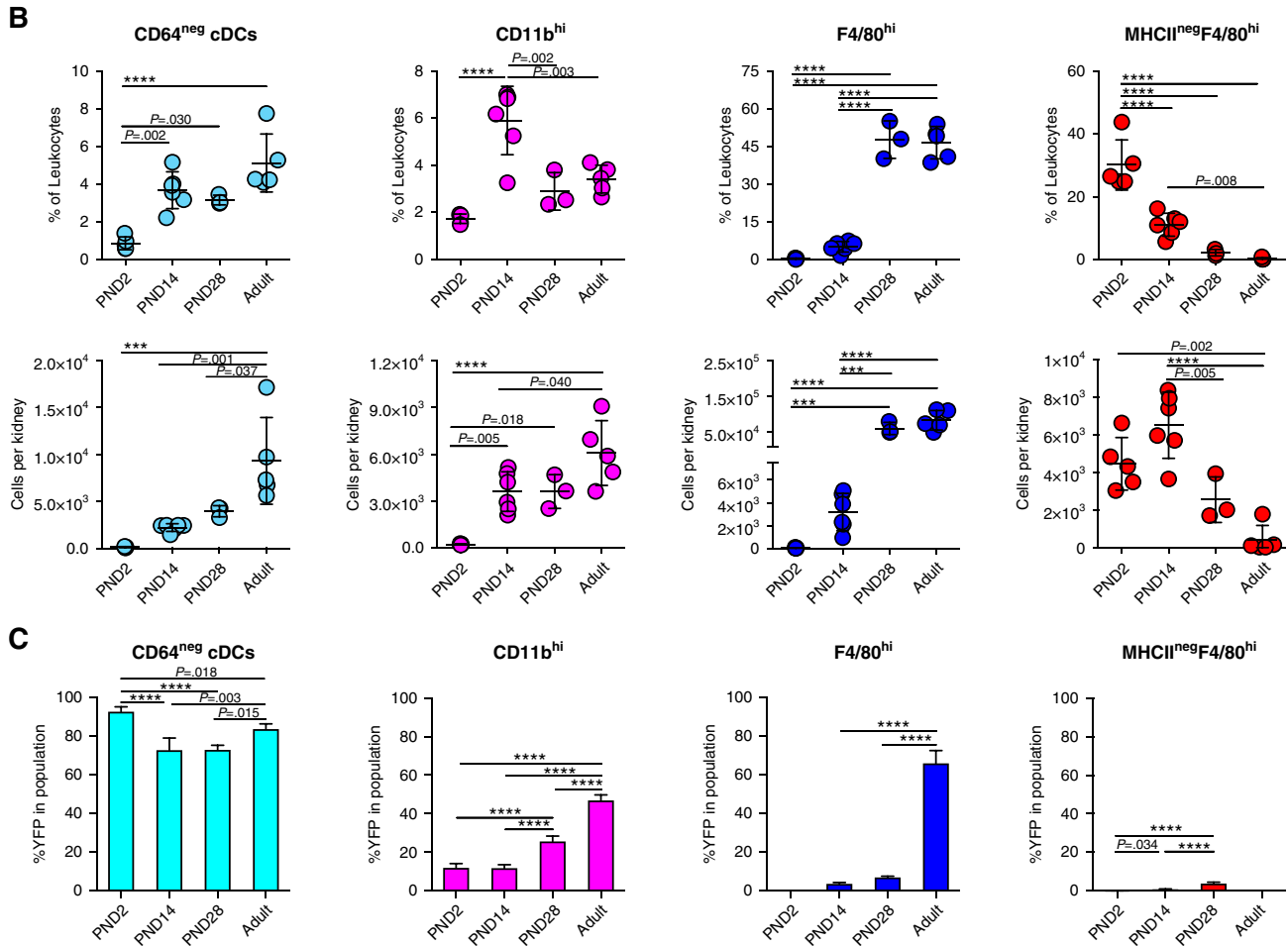
B

C

Figure 4. Continued.

later (Figure 6, Supplemental Figure 5). As in steady state, MHCII⁺ renal leukocytes contained cDC1, cDC2, CD11bhi, and F4/80hi DC populations, with prominent *Clec9a*-expression history, as well as B cells (Figure 6, B–D). Interestingly, upon cisplatin treatment, a small population of MHCIInegF4/80hi cells was found in kidneys from *Clec9acre/creRosaYFP* mice (Figure 6B) and these cells labeled with YFP to the same extent as their MHCII⁺ counterparts (55%±10% versus 62%±10%, respectively; Figure 6, C and D). MHCIIneg and MHCII⁺F4/80hi cells were found in the cortex and medulla, although the renal cortex showed increased signs of apoptosis as measured by cleaved caspase-3 staining and indicative of higher tissue damage in this area (Figure 6, E and F). YFP labeling in other leukocytes, including MHCIInegCD11b⁺ cells that include Ly6G⁺ neutrophils, Ly6C⁺ monocytes, and some Ly6Cint/low cells, remained <5% (Figure 6, B–D, Supplemental Figure 5A). When identifying renal F4/80hi cells independent of MHCII expression, we found lower levels of MHCII expression on F4/80hi cells from cisplatin compared with control-treated mice (Supplemental Figure 5B). Thus, MHCIInegF4/80hi cells that arise after cisplatin injury appear related to the DC lineage and we reasoned that they may be the result of MHCII downregulation from

renal F4/80hi cells, as has been observed in a model of ischemia-reperfusion injury.[35] Three days after subjecting *Clec9acre/creRosaYFP* mice to unilateral ischemia-reperfusion injury, YFP expression remained restricted to DCs (Figure 6G, Supplemental Figure 5C). Notably, MHCIInegF4/80hi cells were found in ischemic kidneys and labeled with YFP at 33%±10% (Figure 6H, Supplemental Figure 5, C and D), although labeling of MHCII⁺F4/80hi cells from the same kidney (57%±10%) or nonischemic kidneys from the same mouse (69%±8%) was higher (Figure 6H). Labeling of monocytes remained low (2%±2%; Figure 6H, Supplemental Figure 5D). These data confirm a DC contribution to MHCIInegF4/80hi cells after ischemia reperfusion, although in this model an additional cell type without *Clec9a*-expression history also appears to contribute.

Renal F4/80hi Leukocytes Transcriptionally Downregulate MHCII Expression after Cisplatin Treatment and Show Altered Expression of Inflammatory Chemokines

To gain a better understanding of the mechanism of MHCII downregulation from F4/80hi cells after cisplatin-induced
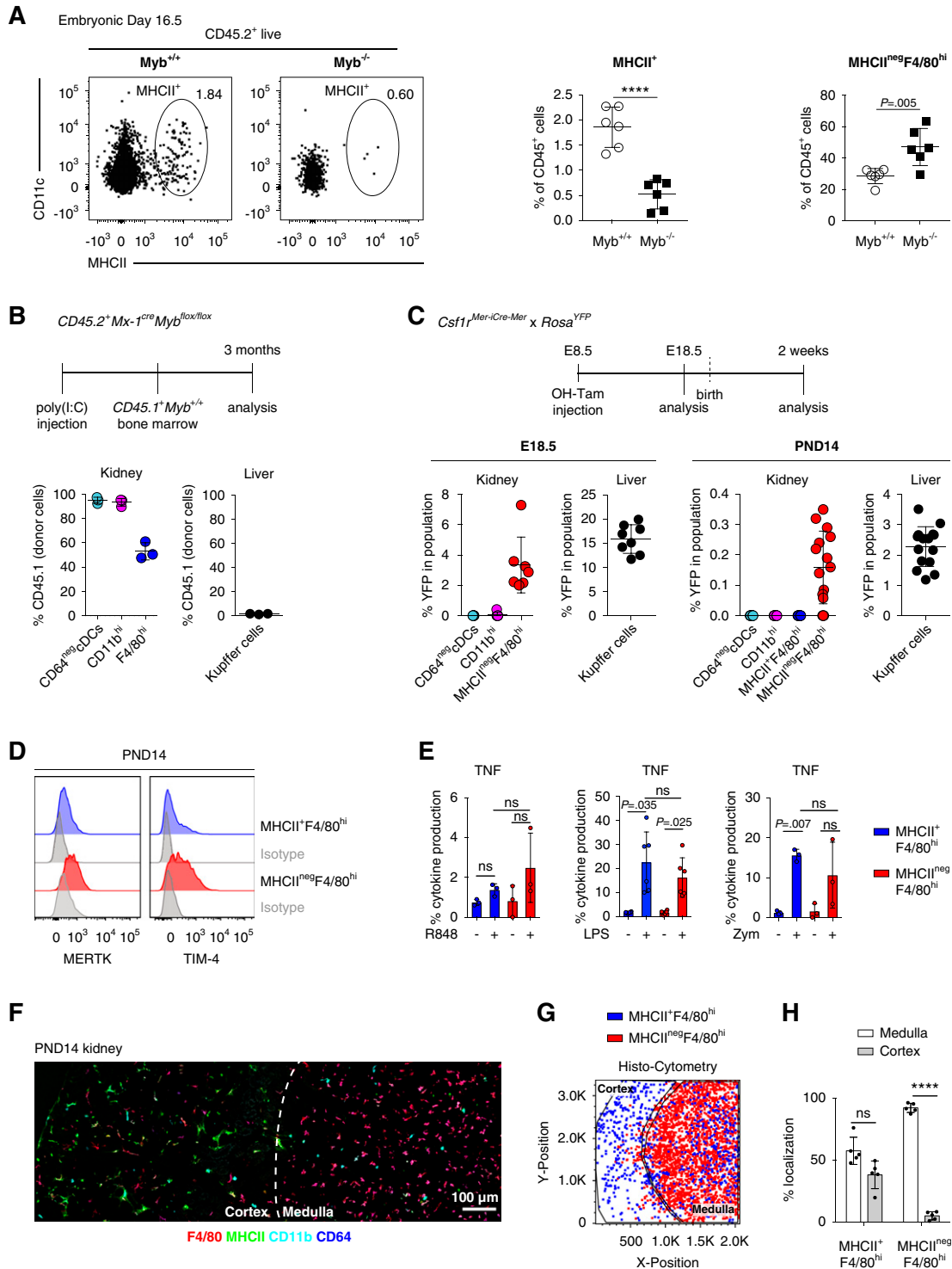
Figure 5. MHCII+ cells in the kidney are *Myb* dependent and do not arise from embryonic progenitors. (A) Kidneys from *Myb−/−* and wild-type littermate control mice were analyzed by flow cytometry on E16.5. Left: CD11c and MHCII expression of live CD45.2+ cells in mouse embryos of the indicated genotype is shown. Right: The frequency of MHCII+ and MHCIInegF4/80hi cells among live CD45.2+ cells is shown. (B) CD45.2+Mx-1creMybflox/flox were treated with serial polyI:C injections to induce deletion of HSCs and subsequently transplanted with bone marrow from congenic CD45.1+ wild-type mice. The percentage of donor-derived CD45.1+ cells in the indicated populations in the liver and kidney is shown. (C) Csf1rMer-iCre-Mer females were mated with male Rosa+/YFP mice and injected with 4-hydroxytamoxifen (OH-TAM) on E8.5. On E18.5 and 2 weeks after birth, kidneys and liver from offspring mice were analyzed for YFP expression by flow cytometry. Renal populations were identified as in Figure 4A. Liver Kupffer cells were identified

AKI, we performed transcriptional analysis of MHCII$^+$F4/80^{hi} and MHCII^{neg}F4/80^{hi} cells from cisplatin-treated mice and MHCII$^+$F4/80^{hi} cells from control-treated mice (Figure 7, Supplemental Figure 6, Supplemental Tables 4–6). PCA revealed the strongest variance between populations from control and cisplatin-treated mice (Figure 7A). Genes involved in antigen presentation—including MHCII, CD74 (invariant chain), and the master regulator of MHCII expression *Ciita*—showed higher expression in MHCII$^+$ than MHCII^{neg}F4/80^{hi} cells from cisplatin-treated mice (Figure 7, B–D), indicating that the antigen-presentation machinery is transcriptionally repressed after cisplatin treatment. Notably, when compared with F4/80^{hi} cells from control-injected mice, MHCII$^+$F4/80^{hi} cells from cisplatin-treated mice showed reduced levels of positive regulators of MCHII expression, including *Ciita*, *Irf4*, *Stat1*, *Irf1*, *Ep300*, and *Creb1*,[60] as well as increased expression of *Cepdb* and *Cebpd*, which inhibit *Ciita* promoter activity.[61] *Cepdb* and *Cebpd* regulate *Ciita* transcription downstream of PGE2 signaling.[62] Notably, renal F4/80^{hi} cells upregulated the PGE2 receptors *Ptger2* (EP2) and *Ptger4* (EP4) in response to cisplatin treatment (Figure 7D), suggesting PG signaling may be involved in mediating MHCII downregulation. Interestingly, renal F4/80^{hi} cells from control and cisplatin-treated mice showed differential expression of several inflammatory chemokines, such as *Ccl2*, *Ccl7*, *Ccl17*, *Cxcl2*, and *Cxcl14* (Figure 7C), indicating these cells may play a role in coordinating recruitment of inflammatory cells. Importantly, renal F4/80^{hi} cells show no evidence of *Clec9a* expression after cisplatin treatment (Supplemental Table 4), further supporting that YFP expression does not result from *de novo* expression of this marker, for instance on infiltrating monocytes (Figure 6, B and D).

DISCUSSION

The origin of kidney MPs has been highly debated because of the large phenotypic overlap of macrophages and DCs in this tissue.[63,64] Adult kidney contains at least four subsets of MPs with prominent *Clec9a*-expression history, indicative of DC origin.[24] These include the main cDC1 and cDC2 subsets, as well as CD64-expressing CD11b^{hi} and F4/80^{hi} cells. Here we show that these populations are phenotypically, functionally, and transcriptionally distinct from each other, suggesting they

may constitute distinct DC subsets. Of these, renal F4/80^{hi} cells have been suggested to constitute macrophages[24,32,30,33] as well as DCs.[24,31] We further demonstrate that renal F4/80^{hi} cells exhibit a unique age-dependent developmental heterogeneity. Kidneys from newborn mice contain a prominent population of macrophages derived from YS erythro-myeloid progenitor that exhibit an F4/80^{hi}CD11b^{low} surface phenotype, express TIM-4 and MERTK, but lack MHCII expression. We show that renal YS erythro-myeloid progenitor–derived macrophages persist only for a few weeks after birth, when they are replaced by phenotypically similar cells that can be distinguished by MHCII expression and a relative lack of TIM-4 and MERTK. *Csf1r*$^{Mer-iCre-Mer}$–mediated fate mapping of YS progenitors demonstrates that MHCII^{neg}F4/80^{hi} and MHCII$^+$F4/80^{hi} cells are ontogenetically distinct cell lineages because YFP labeling in this model is restricted to MHCII^{neg}F4/80^{hi} cells, indicating that YS-derived MHCII^{neg}F4/80^{hi} cells do not acquire MHCII expression with time.

Mx-1^{Cre}*Myb*$^{flox/flox}$ bone marrow rescue chimeras were used to demonstrate replenishment of MHCII$^+$F4/80^{hi} cells from HSCs in adults.[12,44] It has recently been suggested that *Mx-1*^{Cre}*Myb*$^{flox/flox}$ bone marrow rescue chimeras may not mimic steady-state cell differentiation in the kidney as polyI:C treatment induces inflammatory changes in renal leukocyte populations.[35] Why systemic inflammation would induce a loss of resident leukocyte populations in specific tissues is unclear, but it is possible that polyI:C mediates this effect by acting directly on renal epithelial cells.[65] We find a substantial increase in donor chimerism of F4/80^{hi} cells between 3 and 9 months after bone marrow reconstitution. It is likely that, at 9 months after insult, niche-specific inflammatory effects of polyI:C treatment have subsided, substantiating the conclusion that F4/80^{hi} cells are maintained by a low-level, steady-state input from HSCs.

Clec9a-Cre–mediated fate mapping further suggests that MHCII$^+$F4/80^{hi} cells exhibit age-dependent developmental heterogeneity. These cells show *Clec9a*-expression history in adult but not young mice, when compared with CD64^{neg} cDCs, which labeled with YFP at both ages; indicating that DC progenitors contribute to F4/80^{hi} cells in adulthood but not early life. Because *Clec9a-cre*–mediated fate mapping has some limitations, this interpretation needs to be approached with caution. Some DC precursors escape labeling in *Clec9a-Cre*

---

as live CD45.2$^+$F4/80^{hi} cells. The percentage of YFP-positive cells in the indicated populations in kidneys and liver is shown. (D) Renal MHCII$^+$F4/80^{hi} and MHCII^{neg}F4/80^{hi} cells from 2-week-old mice were analyzed for MERTK and TIM-4 expression by flow cytometry. Gray traces represent staining with isotype-matched control antibodies. (E) Renal leukocytes from 2-week-old mice were stimulated *in vitro* with R848, LPS, or zymosan (Zym) for 6 hours and analyzed for intracellular TNF production by flow cytometry. The frequency of TNF-positive MHCII$^+$F4/80^{hi} and MHCII^{neg}F4/80^{hi} cells was calculated and plotted. (F–H) Kidney sections from two-week-old *Clec9a*^{cre}*Rosa*^{Tom} mice were analyzed by histo-cytometry. (F) Immunofluorescence image of the following markers: F4/80 (red), MHCII (green), CD11b (magenta), and CD64 (blue). Scale bar, 100 μm. (G) Histo-cytometry was used to identify the x and y position of MHCII^{neg}F4/80^{hi} and MHCII$^+$F4/80^{hi} cells in the kidney sections. Lines separating renal medulla and cortex were drawn by hand based on tissue structure, autofluorescence properties, and presence of glomeruli. (H) The frequency of MHCII^{neg} F4/80^{hi} and MHCII$^+$F4/80^{hi} cells located in the renal cortex and medulla was quantified using gates on the renal cortex or medulla in histo-cytometry analysis and plotted. Each dot represents one mouse. Horizontal bars represent mean, error bars represent SD. ****$P < 0.0001$.
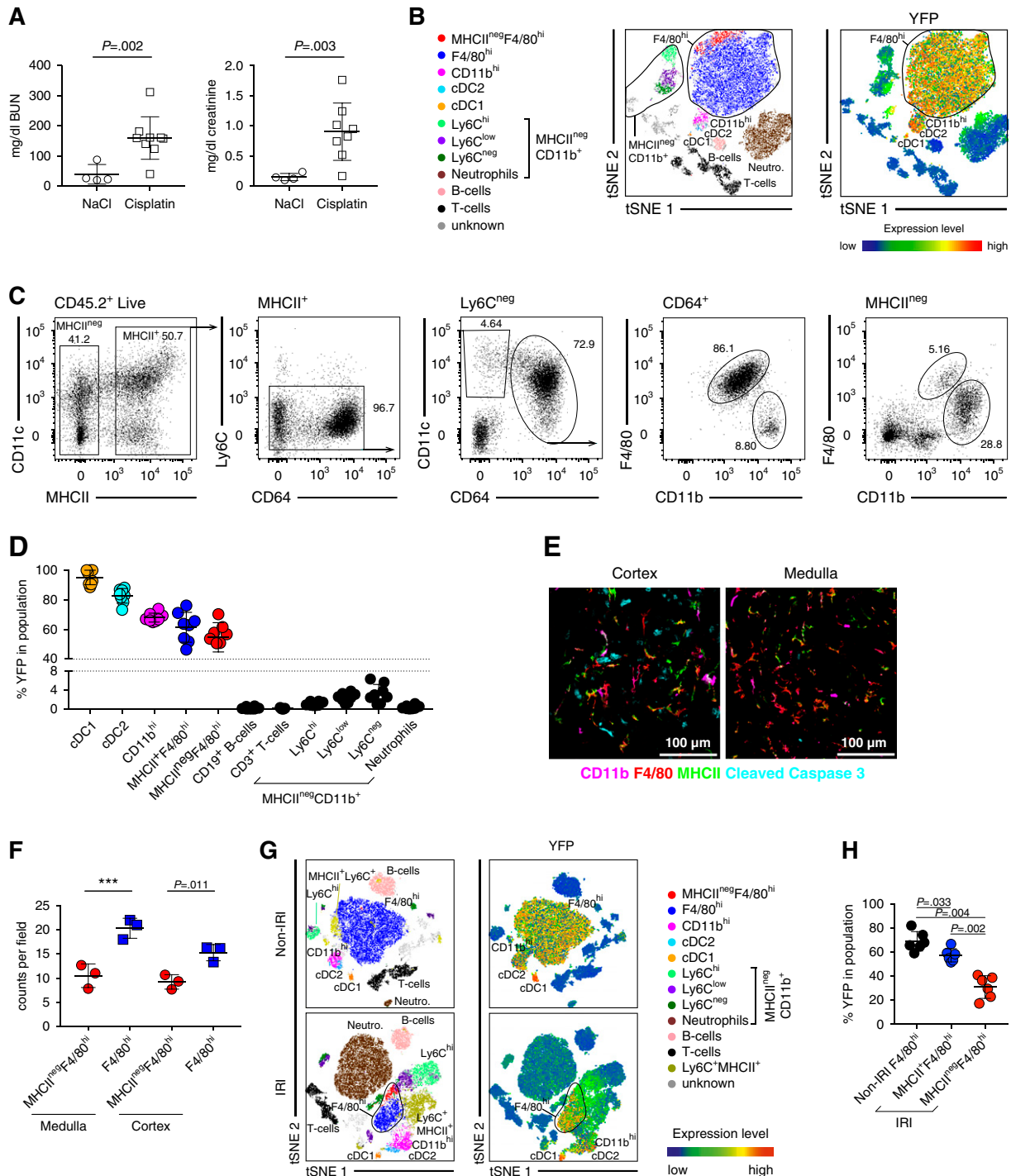
Figure 6. Renal MHCII[neg]F4/80^{hi} cells appear in adult kidneys after cisplatin and ischemia-induced AKI due to a phenotypic switch of MHCII[+]F4/80^{hi} cells. (A–D) *Clec9a[cre/cre]Rosa[YFP]* mice, 10 weeks of age, were injected i.p. with 15 mg/kg cisplatin and analyzed 72 hours later. (A) Serum creatinine and BUN levels are shown. (B–D) Kidney leukocytes from cisplatin-treated *Clec9a[cre/cre]Rosa[YFP]* mice were analyzed by flow cytometry. (B) Representative tSNE analysis of kidney leukocytes 3 days after cisplatin treatment. Left panel: Cells were clustered independently of YFP labeling and manually gated populations were overlaid on the tSNE plot in the indicated colors. Right panel: The intensity of YFP expression in the indicated populations. Blue-to-red gradient indicates level of marker expression. (C and D) CD45.2^{+} cells were subdivided into MHCII^{neg} and MHCII^{+} cells. MHCII^{+} cells were further analyzed for CD11c and CD64 expression. After exclusion of Ly6C^{neg} cells, MHCII^{+}CD64^{+} cells (first row) and MHCII^{neg} cells (second row) were further analyzed for CD11b and F4/80 expression. (D) The percentage of YFP^{+} labeling in the indicated renal leukocyte populations from cisplatin-treated mice is shown. (E) Kidney sections from cisplatin-treated mice were analyzed by immunofluorescence microscopy for the following

mice and therefore YFP expression needs to be considered at the population level and no definitive conclusion can be made about the origin of YFP-negative cells.[24] Incomplete penetrance of CRE-mediated DNA rearrangement could explain the lack of obvious transcriptional differences between YFP⁻ and YFP⁺ F4/80hi cells in adults. However, it is important to note that a failure to detect transcriptional differences in ontogenetically distinct cell types could also be due to environmental imprinting.[66,67] The transcriptional resemblance of MHCII⁺F4/80hi cells to macrophages in adult mice may additionally raise some doubt about the lineage-restricted expression of *Clec9a*. However, in steady state as well as in inflammation, *Clec9a*-expression history does not exceed a 5% background level in other lymphoid or myeloid cells, including monocytes, which are putative progenitors of MHCII⁺F4/80hi cells in other tissues (Figures 1B and 6D, Supplemental Figure 5D). These data strongly support that *Clec9a* expression is DC-lineage restricted.[24,68] Additionally, we have not found evidence of *Clec9a* promoter activity in renal F4/80hi cells in steady state and after renal inflammation (Supplemental Figure 2C, Supplemental Table 4),[24] indicating that renal MHCII⁺F4/80hi cells do not acquire *Clec9a* expression in their differentiated state. Thus, despite possible caveats of *Clec9a*-Cre–mediated fate mapping, the age-dependent differences in *Clec9a*-expression history of MCHII⁺F4/80hi cells strongly suggest a distinct origin of MCHII⁺F4/80hi cells in early and adult life. Notably, YFP labeling also suggests an age-dependent heterogeneity of CD11bhi cells. Because monocytes and lymphoid progenitors can contribute to macrophage and DC-like cells,[1,11,17,69–71] these cells could also be putative progenitors of CD11bhi and F4/80hi cells in early life, which needs to be investigated.

Layered development of immune cells has been demonstrated across tissues, although we are just beginning to decipher the functional consequences of this ontogenetic diversity.[5,6,72] Because kidney development in mice is not complete at birth, it is possible that renal macrophage and DC development is coordinated in distinct developmental waves to accommodate unique phases in organ growth and physiology, as well as an increasing need for immune defense with age. Our observation that MHCII⁺F4/80hi and MHCIInegF4/80hi cells from 2-week-old mice respond to TLR ligands with lower TNF production than their adult counterparts implies that

F4/80hi cells in early life may have lower inflammatory capacity than in adulthood. Whether such age-dependent functional differences are rooted in distinct cell ontogeny or are secondary to environmental differences between young and adult mice[73,74] needs to be investigated. The differential expression of MHCII on YS and HSC-derived F4/80hi cells further implies differences in antigen presentation and T cell activation, and the preferential localization of MHCIInegF4/80hi YS-derived macrophages in medulla from 2-week-old mice could place these cells in position to defend against ascending pathogens, as has been described for adult medullary DCs.[31] Macrophages favorably influence kidney growth through apoptotic cell uptake and by promoting vascularization.[75,76] Intriguingly however, unlike in other organs where self-maintaining MHCIIneg macrophages promote vascular integrity and tissue repair in adulthood,[19,77] MHCIInegF4/80hi cells are not found in steady-state adult kidney, although the kidney is highly vascularized. It is possible that MHCII⁺F4/80hi cells from adult kidney have a unique role in antigen presentation, because circulating antigens are constitutively filtered and concentrated in the kidney and these cells can induce T cell activation and effector differentiation *in vitro*.[24]

Particularly intriguing are our findings that, in response to AKI, MHCIInegF4/80hi cells appear in kidneys that show prominent YFP labeling in *Clec9aCreRosaYFP* mice. We demonstrate that YFP expression remains restricted to the DC lineage after renal inflammation and no labeling is observed in other lymphoid and myeloid lineages, including monocytes. These data strongly support a DC origin of MHCIInegF4/80hi cells. Although it is possible that MHCIInegF4/80hi cells result from *de novo* differentiation of *Clec9a*-expressing progenitors that enter the tissue, we do not believe this is the case because transcriptional profiling indicates that F4/80hi cells shut off MHCII transcription in response to cisplatin. These data are consistent with a recent study reporting downregulation of MHCII on renal F4/80hi cells 6 days after bilateral ischemia-reperfusion injury.[35] Our data further suggest that MHCII expression may be regulated by PGE2, which is produced by renal tubular cells after cisplatin treatment.[78] Because MHCIIneg macrophages have been implicated in wound healing,[35,55,77] it is possible that kidney-resident F4/80hi cells respond to inflammation by contributing to tissue repair, possibly coordinating the

markers: CD11b (magenta), F4/80 (red), MHCII (green), and cleaved caspase-3 (cyan). Representative cutouts of renal cortex and medulla are shown. Scale bar, 100 μm. (F) Quantification of MHCII⁺F4/80hi and MHCIInegF4/80hi cells in the renal cortex and medulla in cisplatin-treated mice. Each dot represents the average amount of cells per field from one biologic replicate. (G and H) FACS analysis of renal leukocytes from *Clec9acre/creRosaYFP* mouse 72 hours after unilateral ischemia-reperfusion injury. (G) Representative tSNE analyses of kidney leukocytes from ischemic and nonischemic control kidneys. Left panel: Cells were clustered independently of YFP labeling and manually gated populations were overlaid on the tSNE plot in the indicated colors. Right panel: YFP expression in the indicated populations. Blue-to-red gradient indicates increasing intensity of marker expression. (H) The percentage of YFP⁺ cells in renal MHCII⁺F4/80hi cells from nonischemic control kidneys and MHCIIneg and MHCII⁺F4/80hi cells from ischemic kidneys is shown. Each dot represents one mouse. Horizontal bars represent mean, error bars represent SD. ***$P<0.001$. IRI, ischemic-reperfusion injury; NaCl, sodium chloride.
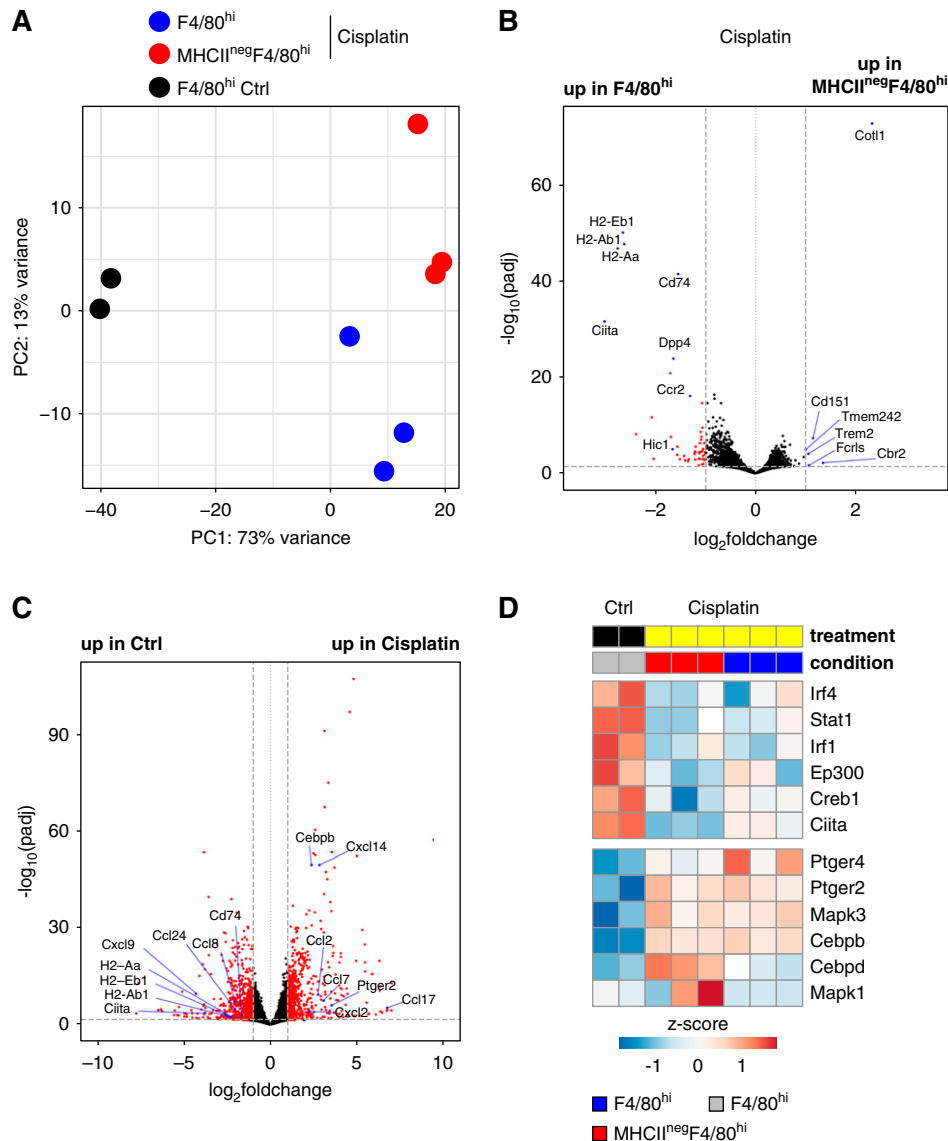
Figure 7. Renal F4/80^hi cells downregulate MHCII expression and induce inflammatory chemokine expression in response to cisplatin treatment. At 72 hours after cisplatin treatment, MHCII^+F4/80^hi and MHCII^negF4/80^hi cells were sorted from 10-week-old C57BL/6J mice and subjected to mRNA-sequencing analysis. As control (Ctrl), MHCII^+F4/80^hi cells were sorted from sodium chloride–injected mice. (A) PCA of the top 5000 genes with highest variance across all samples. Each dot of the same color represents a biologic replicate. (B) Pairwise comparison of MHCII^+F4/80^hi and MHCII^negF4/80^hi populations from cisplatin-treated mice. (C) Pairwise comparison of F4/80^hi populations from control and cisplatin-treated mice independent of MHCII expression. Red circles indicate genes with a log₂ fold change greater than one between samples and an adjusted *P* (padj) value of <0.05. (D) Heatmap of genes implicated in inducing (upper block) or repressing (lower block) MHCII expression.

trafficking of other immune cells in the kidney through the production of chemokines.

Future studies are necessary to decipher the tissue-specific signals that regulate age-dependent aspects of DC and macrophage development in the kidney. Because the kidney is not a barrier organ, the microbiota is unlikely to play a role. However, the distinct salt environment of the kidney could influence hematopoietic programs, for instance by functional imprinting or modulating the recruitment of progenitor cells.[79,80] Understanding age-dependent developmental aspects of long-lived,

tissue-resident MPs with putative immune-modulatory and antigen-presenting function has important implications for targeting these cells for therapeutic intervention.

We acknowledge the Core Facility Flow Cytometry and the Core Facility Bioimaging at the Biomedical Center, Ludwig Maximilian University of Munich for providing equipment and expertise. High throughput sequencing was performed by the Laboratory for Functional Genome Analysis of the LMU Munich.

Dr. Salei, Mr. Rambichler, and Dr. Schraml planned experiments and wrote the manuscript. Dr. Salei, Mr. Rambichler, Ms. J. Salvermoser, Mr. Papaioannou, Dr. Schuchert, Dr. Cernilogar, Ms. Li, Mr. Marschner, and Dr. Schraml performed experiments. Mr. Rambichler, Dr. Straub, and Dr. Schotta performed sequencing analysis. Dr. Pakalniškytė, Mr. Rambichler, and Dr. Salei optimized the protocol for AKI. Dr. M. Salvermoser and Dr. Walzog helped with migration assays. Dr. Stremmel, Dr. Anders, Dr. Lichtnekert, and Dr. Schotta provided valuable intellectual input. Dr. Schraml designed and supervised the study.

DISCLOSURES

FUNDING

SUPPLEMENTAL MATERIAL

This article contains the following supplemental material online at http://jasn.asnjournals.org/lookup/suppl/doi:10.1681/ASN.2019040419/-/DCSupplemental.

Supplemental Figure 1. *Clec9a-Cre* mice faithfully trace renal dendritic cells.

Supplemental Figure 2. Gating strategy and sort purity of YFP$^+$ and YFP$^-$ F4/80^{hi} and CD11b^{hi} cells from kidney.

Supplemental Figure 3. Cytokine production in renal YFP$^+$ and YFP$^-$ F4/80^{hi} and YFP$^+$ and YFP$^-$ CD11b^{hi} cells after TLR ligand stimulation.

Supplemental Figure 4. MHCII$^+$ cells in the kidney are *Myb*-dependent and do not arise from embryonic progenitors.

Supplemental Figure 5. Leukocyte gating strategy and fate mapping of DCs in cisplatin- and ischemia- reperfusion-induced AKI.

Supplemental Figure 6. Gating strategy and sort purity of F4/80^{hi} and MHCII^{neg}F4/80^{hi} cells after cisplatin-induced AKI.

Supplemental Table 1. Differentially expressed genes between F4/80^{hi} YFP$^+$, CD11b^{hi} YFP$^+$, cDC2 and cDC1 analyzed with DESeq2 and used for k-means clustering.

Supplemental Table 2. Differentially expressed genes between cDC2 YFP$^+$ and CD11b^{hi} YFP$^+$ analyzed with DESeq2.

Supplemental Table 3. Differentially expressed genes between F4/80^{hi} YFP$^+$ and CD11b^{hi} YFP$^+$ analyzed with DESeq2.

Supplemental Table 4. TPM values of RNAseq from MHCII$^{+/neg}$ F4/80^{hi} cells after cisplatin-induced AKI.

Supplemental Table 5. Differentially expressed genes between MHCII^{neg}F4/80^{hi} and MHCII$^+$F4/80^{hi} after cisplatin-induced AKI analyzed with DESeq2.

Supplemental Table 6. Differentially expressed genes between F4/80^{hi} cells and F4/80^{hi} cells after cisplatin-induced AKI analyzed with DESeq2.

REFERENCES

1. Guilliams M, Ginhoux F, Jakubzick C, Naik SH, Onai N, Schraml BU, et al.: Dendritic cells, monocytes and macrophages: A unified nomenclature based on ontogeny. *Nat Rev Immunol* 14: 571–578, 2014

2. Merad M, Sathe P, Helft J, Miller J, Mortha A: The dendritic cell lineage: Ontogeny and function of dendritic cells and their subsets in the steady state and the inflamed setting. *Annu Rev Immunol* 31: 563–604, 2013

3. Murphy TL, Grajales-Reyes GE, Wu X, Tussiwand R, Briseño CG, Iwata A, et al.: Transcriptional control of dendritic cell development. *Annu Rev Immunol* 34: 93–119, 2016

4. Mildner A, Yona S, Jung S: A close encounter of the third kind: Monocyte-derived cells. *Adv Immunol* 120: 69–103, 2013

5. Ginhoux F, Jung S: Monocytes and macrophages: Developmental pathways and tissue homeostasis. *Nat Rev Immunol* 14: 392–404, 2014

6. Ginhoux F, Guilliams M: Tissue-resident macrophage ontogeny and homeostasis. *Immunity* 44: 439–449, 2016

7. Jenkins SJ, Hume DA: Homeostasis in the mononuclear phagocyte system. *Trends Immunol* 35: 358–367, 2014

8. Ginhoux F, Greter M, Leboeuf M, Nandi S, See P, Gokhan S, et al.: Fate mapping analysis reveals that adult microglia derive from primitive macrophages. *Science* 330: 841–845, 2010

9. Palis J, Robertson S, Kennedy M, Wall C, Keller G: Development of erythroid and myeloid progenitors in the yolk sac and embryo proper of the mouse. *Development* 126: 5073–5084, 1999

10. Bertrand JY, Jalil A, Klaine M, Jung S, Cumano A, Godin I: Three pathways to mature macrophages in the early mouse yolk sac. *Blood* 106: 3004–3011, 2005

11. Hoeffel G, Chen J, Lavin Y, Low D, Almeida FF, See P, et al.: C-Myb(+) erythro-myeloid progenitor-derived fetal monocytes give rise to adult tissue-resident macrophages. *Immunity* 42: 665–678, 2015

12. Schulz C, Gomez Perdiguero E, Chorro L, Szabo-Rogers H, Cagnard N, Kierdorf K, et al.: A lineage of myeloid cells independent of Myb and hematopoietic stem cells. *Science* 336: 86–90, 2012

13. Perdiguero EG, Klapproth K, Schulz C, Busch K, Azzoni E, Crozet L, et al.: Tissue-resident macrophages originate from yolk-sac-derived erythro-myeloid progenitors. *Nature Publishing Group* 518: 1–17, 2014

14. Gentek R, Molawi K, Sieweke MH: Tissue macrophage identity and self-renewal. *Immunol Rev* 262: 56–73, 2014

15. Mossadegh-Keller N, Gentek R, Gimenez G, Bigot S, Mailfert S, Sieweke MH: Developmental origin and maintenance of distinct testicular macrophage populations. *J Exp Med* 214: 2829–2841, 2017

16. Epelman S, Lavine KJ, Beaudin AE, Sojka DK, Carrero JA, Calderon B, et al.: Embryonic and adult-derived resident cardiac macrophages are

maintained through distinct mechanisms at steady state and during inflammation. *Immunity* 40: 91–104, 2014

17. Bain CC, Bravo-Blas A, Scott CL, Perdiguero EG, Geissmann F, Henri S, et al.: Constant replenishment from circulating monocytes maintains the macrophage pool in the intestine of adult mice. *Nat Immunol* 15: 929–937, 2014

18. Shaw TN, Houston SA, Wemyss K, Bridgeman HM, Barbera TA, Zangerle-Murray T, et al.: Tissue-resident macrophages in the intestine are long lived and defined by Tim-4 and CD4 expression. *J Exp Med* 215: 1507–1518, 2018

19. De Schepper S, Verheijden S, Aguilera-Lizarraga J, Viola MF, Boesmans W, Stakenborg N, et al.: Self-maintaining gut macrophages are essential for intestinal homeostasis. *Cell* 175: 400–415.e13, 2018

20. Fogg DK, Sibon C, Miled C, Jung S, Aucouturier P, Littman DR, et al.: A clonogenic bone marrow progenitor specific for macrophages and dendritic cells. *Science* 311: 83–87, 2006

21. Naik SH, Sathe P, Park H-Y, Metcalf D, Proietto AI, Dakic A, et al.: Development of plasmacytoid and conventional dendritic cell subtypes from single precursor cells derived in vitro and in vivo. *Nat Immunol* 8: 1217–1226, 2007

22. Onai N, Obata-Onai A, Schmid MA, Ohteki T, Jarrossay D, Manz MG: Identification of clonogenic common Flt3+M-CSFR+ plasmacytoid and conventional dendritic cell progenitors in mouse bone marrow. *Nat Immunol* 8: 1207–1216, 2007

23. Ginhoux F, Liu K, Helft J, Bogunovic M, Greter M, Hashimoto D, et al.: The origin and development of nonlymphoid tissue CD103+ DCs. *J Exp Med* 206: 3115–3130, 2009

24. Schraml BU, van Blijswijk J, Zelenay S, Whitney PG, Filby A, Acton SE, et al.: Genetic tracing via DNGR-1 expression history defines dendritic cells as a hematopoietic lineage. *Cell* 154: 843–858, 2013

25. Cabeza-Cabrerizo M, van Blijswijk J, Wienert S, Heim D, Jenkins RP, Chakravarty P, et al.: Tissue clonality of dendritic cell subsets and emergency DCpoiesis revealed by multicolor fate mapping of DC progenitors. *Sci Immunol* 4: eaaw1941, 2019

26. Guilliams M, Dutertre C-A, Scott CL, McGovern N, Sichien D, Chakarov S, et al.: Unsupervised high-dimensional analysis aligns dendritic cells across tissues and species. *Immunity* 45: 669–684, 2016

27. Langlet C, Tamoutounour S, Henri S, Luche H, Ardouin L, Grégoire C, et al.: CD64 expression distinguishes monocyte-derived and conventional dendritic cells and reveals their distinct role during intramuscular immunization. *J Immunol* 188: 1751–1760, 2012

28. Tamoutounour S, Henri S, Lelouard H, de Bovis B, de Haar C, van der Woude CJ, et al.: CD64 distinguishes macrophages from dendritic cells in the gut and reveals the Th1-inducing role of mesenteric lymph node macrophages during colitis. *Eur J Immunol* 42: 3150–3166, 2012

29. Brähler S, Zinselmeyer BH, Raju S, Nitschke M, Suleiman H, Saunders BT, et al.: Opposing roles of dendritic cell subsets in experimental GN. *J Am Soc Nephrol* 29: 138–154, 2018

30. Lionakis MS, Swamydas M, Fischer BG, Plantinga TS, Johnson MD, Jaeger M, et al.: CX3CR1-dependent renal macrophage survival promotes Candida control and host survival. *J Clin Invest* 123: 5035–5051, 2013

31. Hochheiser K, Heuser C, Krause TA, Teteris S, Ilias A, Weisheit C, et al.: Exclusive CX3CR1 dependence of kidney DCs impacts glomerulonephritis progression. *J Clin Invest* 123: 4242–4254, 2013

32. Cao Q, Wang Y, Wang XM, Lu J, Lee VWS, Ye Q, et al.: Renal F4/80+ CD11c+ mononuclear phagocytes display phenotypic and functional characteristics of macrophages in health and in adriamycin nephropathy. *J Am Soc Nephrol* 26: 349–363, 2015

33. Stamatiades EG, Tremblay M-E, Bohm M, Crozet L, Bisht K, Kao D, et al.: Immune monitoring of trans-endothelial transport by kidney-resident macrophages. *Cell* 166: 991–1003, 2016

34. Lever JM, Yang Z, Boddu R, Adedoyin OO, Guo L, Joseph R, et al.: Parabiosis reveals leukocyte dynamics in the kidney. *Lab Invest* 98: 391–402, 2018

35. Lever JM, Hull TD, Boddu R, Pepin ME, Black LM, Adedoyin OO, et al.: Resident macrophages reprogram toward a developmental state after acute kidney injury. *JCI Insight* 4: 833, 2019

36. Puranik AS, Leaf IA, Jensen MA, Hedayat AF, Saad A, Kim K-W, et al.: Kidney-resident macrophages promote a proangiogenic environment in the normal and chronically ischemic mouse kidney. *Sci Rep* 8: 13948, 2018

37. Srinivas S, Watanabe T, Lin CS, William CM, Tanabe Y, Jessell TM, et al.: Cre reporter strains produced by targeted insertion of EYFP and ECFP into the ROSA26 locus. *BMC Dev Biol* 1: 4, 2001

38. Madisen L, Zwingman TA, Sunkin SM, Oh SW, Zariwala HA, Gu H, et al.: A robust and high-throughput Cre reporting and characterization system for the whole mouse brain. *Nat Neurosci* 13: 133–140, 2010

39. Jung S, Aliberti J, Graemmel P, Sunshine MJ, Kreutzberg GW, Sher A, et al.: Analysis of fractalkine receptor CX(3)CR1 function by targeted deletion and green fluorescent protein reporter gene insertion. *Mol Cell Biol* 20: 4106–4114, 2000

40. Mucenski ML, McLain K, Kier AB, Swerdlow SH, Schreiner CM, Miller TA, et al.: A functional c-myb gene is required for normal murine fetal hepatic hematopoiesis. *Cell* 65: 677–689, 1991

41. Qian B-Z, Li J, Zhang H, Kitamura T, Zhang J, Campion LR, et al.: CCL2 recruits inflammatory monocytes to facilitate breast-tumour metastasis. *Nature* 475: 222–225, 2011

42. Kühn R, Schwenk F, Aguet M, Rajewsky K: Inducible gene targeting in mice. *Science* 269: 1427–1429, 1995

43. Lieu YK, Kumar A, Pajerowski AG, Rogers TJ, Reddy EP: Requirement of c-myb in T cell development and in mature T cell function. *Proc Natl Acad Sci U S A* 101: 14853–14858, 2004

44. Stremmel C, Schuchert R, Schneider V, Weinberger T, Thaler R, Messerer D, et al.: Inducible disruption of the c-myb gene allows allogeneic bone marrow transplantation without irradiation. *J Immunol Methods* 457: 66–72, 2018

45. Marschner JA, Schäfer H, Holderied A, Anders H-J: Optimizing mouse surgery with online rectal temperature monitoring and preoperative heat supply. Effects on post-ischemic acute kidney injury. *PLoS One* 11: e0149489, 2016

46. Dobin A, Davis CA, Schlesinger F, Drenkow J, Zaleski C, Jha S, et al.: STAR: Ultrafast universal RNA-seq aligner. *Bioinformatics* 29: 15–21, 2013

47. Li B, Dewey CN: RSEM: Accurate transcript quantification from RNA-Seq data with or without a reference genome. *BMC Bioinformatics* 12: 323, 2011

48. Zhu A, Ibrahim JG, Love MI: Heavy-tailed prior distributions for sequence count data: Removing the noise and preserving large differences. *Bioinformatics* 35: 2084–2092, 2019

49. Bajénoff M, Glaichenhaus N, Germain RN: Fibroblastic reticular cells guide T lymphocyte entry into and migration within the splenic T cell zone. *J Immunol* 181: 3947–3954, 2008

50. Schindelin J, Arganda-Carreras I, Frise E, Kaynig V, Longair M, Pietzsch T, et al.: Fiji: An open-source platform for biological-image analysis. *Nat Methods* 9: 676–682, 2012

51. Li W, Germain RN, Gerner MY: Multiplex, quantitative cellular analysis in large tissue volumes with clearing-enhanced 3D microscopy (C$_e$3D). *Proc Natl Acad Sci U S A* 114: E7321–E7330, 2017

52. Liu J, Willet SG, Bankaitis ED, Xu Y, Wright CVE, Gu G: Non-parallel recombination limits Cre-LoxP-based reporters as precise indicators of conditional genetic manipulation. *Genesis* 51: 436–442, 2013

53. Yona S, Kim K-W, Wolf Y, Mildner A, Varol D, Breker M, et al.: Fate mapping reveals origins and dynamics of monocytes and tissue macrophages under homeostasis. *Immunity* 38: 79–91, 2013

54. Scott CL, Zheng F, De Baetselier P, Martens L, Saeys Y, De Prijck S, et al.: Bone marrow-derived monocytes give rise to self-renewing and fully differentiated Kupffer cells. *Nat Commun* 7: 10321, 2016

55. Dick SA, Macklin JA, Nejat S, Momen A, Clemente-Casares X, Althagafi MG, et al.: Self-renewing resident cardiac macrophages limit adverse remodeling following myocardial infarction. *Nat Immunol* 20: 29–39, 2019

56. Sheng J, Ruedl C, Karjalainen K: Most tissue-resident macrophages except microglia are derived from fetal hematopoietic stem cells. *Immunity* 43: 382–393, 2015

57. Busch K, Klapproth K, Barile M, Flossdorf M, Holland-Letz T, Schlenner SM, et al.: Fundamental properties of unperturbed haematopoiesis from stem cells in vivo. *Nature* 518: 542–546, 2015

58. Gerner MY, Kastenmuller W, Ifrim I, Kabat J, Germain RN: Histo-cytometry: A method for highly multiplex quantitative tissue imaging analysis applied to dendritic cell subset microanatomy in lymph nodes. *Immunity* 37: 364–376, 2012

59. Ramesh G, Ranganathan P: Mouse models and methods for studying human disease, acute kidney injury (AKI). *Methods Mol Biol* 1194: 421–436, 2014

60. Boss JM, Jensen PE: Transcriptional regulation of the MHC class II antigen presentation pathway. *Curr Opin Immunol* 15: 105–111, 2003

61. Pennini ME, Liu Y, Yang J, Croniger CM, Boom WH, Harding CV: CCAAT/enhancer-binding protein beta and delta binding to CIITA promoters is associated with the inhibition of CIITA expression in response to Mycobacterium tuberculosis 19-kDa lipoprotein. *J Immunol* 179: 6910–6918, 2007

62. Li G, Harton JA, Zhu X, Ting JPY: Downregulation of CIITA function by protein kinase a (PKA)-mediated phosphorylation: Mechanism of prostaglandin E, cyclic AMP, and PKA inhibition of class II major histocompatibility complex expression in monocytic lines. *Mol Cell Biol* 21: 4626–4635, 2001

63. Nelson PJ, Rees AJ, Griffin MD, Hughes J, Kurts C, Duffield J: The renal mononuclear phagocytic system. *J Am Soc Nephrol* 23: 194–203, 2012

64. Gottschalk C, Kurts C: The debate about dendritic cells and macrophages in the kidney. *Front Immunol* 6: 435, 2015

65. Hägele H, Allam R, Pawar RD, Anders HJ: Double-stranded RNA activates type I interferon secretion in glomerular endothelial cells via retinoic acid-inducible gene (RIG)-1. *Nephrol Dial Transplant* 24: 3312–3318, 2009

66. Gosselin D, Link VM, Romanoski CE, Fonseca GJ, Eichenfield DZ, Spann NJ, et al.: Environment drives selection and function of enhancers controlling tissue-specific macrophage identities. *Cell* 159: 1327–1340, 2014

67. Lavin Y, Winter D, Blecher-Gonen R, David E, Keren-Shaul H, Merad M, et al.: Tissue-resident macrophage enhancer landscapes are shaped by the local microenvironment. *Cell* 159: 1312–1326, 2014

68. Joffre OP, Sancho D, Zelenay S, Keller AM, Reis e Sousa C: Efficient and versatile manipulation of the peripheral CD4+ T-cell compartment by antigen targeting to DNGR-1/CLEC9A. *Eur J Immunol* 40: 1255–1265, 2010

69. Salvermoser J, van Blijswijk J, Papaioannou NE, Rambichler S, Pasztoi M, Pakalniškytė D, et al.: Clec9a-mediated ablation of conventional dendritic cells suggests a lymphoid path to generating dendritic cells in vivo. *Front Immunol* 9: 563–615, 2018

70. Rodrigues PF, Alberti-Servera L, Eremin A, Grajales-Reyes GE, Ivanek R, Tussiwand R: Distinct progenitor lineages contribute to the heterogeneity of plasmacytoid dendritic cells. *Nat Immunol* 392: 1–18, 2018

71. Audzevich T, Bashford-Rogers R, Mabbott NA, Frampton D, Freeman TC, Potocnik A, et al.: Pre/pro-B cells generate macrophage populations during homeostasis and inflammation. *Proceedings of the National Academy of Sciences* 114: E3954–E3963, 2017

72. Hoeffel G, Ginhoux F: Ontogeny of tissue-resident macrophages. *Front Immunol* 6: 486, 2015

73. de Kleer IM, Kool M, de Bruijn MJW, Willart M, van Moorleghem J, Schuijs MJ, et al.: Perinatal activation of the interleukin-33 pathway promotes type 2 immunity in the developing lung. *Immunity* 45: 1285–1298, 2016

74. Bachus H, Kaur K, Papillion AM, Marquez-Lago TT, Yu Z, Ballesteros-Tato A, et al.: Impaired tumor-necrosis-factor-α-driven dendritic cell activation limits lipopolysaccharide-induced protection from allergic inflammation in infants. *Immunity* 50:225–240.e4, 2019

75. Rae F, Woods K, Sasmono T, Campanale N, Taylor D, Ovchinnikov DA, et al.: Characterisation and trophic functions of murine embryonic macrophages based upon the use of a Csf1r-EGFP transgene reporter. *Dev Biol* 308: 232–246, 2007

76. Munro DAD, Wineberg Y, Tarnick J, Vink CS, Li Z, Pridans C, et al.: Macrophages restrict the nephrogenic field and promote endothelial connections during kidney development. *Elife* 8: e43271, 2019

77. Chakarov S, Lim HY, Tan L, Lim SY, See P, Lum J, et al.: Two distinct interstitial macrophage populations coexist across tissues in specific subtissular niches. *Science* 363: eaau0964, 2019

78. Jia Z, Wang N, Aoyagi T, Wang H, Liu H, Yang T: Amelioration of cisplatin nephrotoxicity by genetic or pharmacologic blockade of prostaglandin synthesis. *Kidney Int* 79: 77–88, 2011

79. Berry MR, Mathews RJ, Ferdinand JR, Jing C, Loudon KW, Wlodek E, et al.: Renal sodium gradient orchestrates a dynamic antibacterial defense zone. *Cell* 170: 860–874.e19, 2017

80. Chessa F, Mathow D, Wang S, Hielscher T, Atzberger A, Porubsky S, et al.: The renal microenvironment modifies dendritic cell phenotype. *Kidney Int* 89: 82–94, 2016

AFFILIATIONS

[1]Walter Brendel Centre of Experimental Medicine, University Hospital Munich, [2]Institute for Cardiovascular Physiology and Pathophysiology, [7]Division of Molecular Biology, [8]Core Facility Bioinformatics, and [9]Center for Integrated Protein Science Munich, Biomedical Center, Faculty of Medicine, Ludwig Maximilian University of Munich, Martinsried, Germany; [3]Medical Clinic and Polyclinic I and [6]Division of Nephrology, Medical Clinic and Polyclinic IV, University Hospital Munich, Ludwig Maximilian University of Munich, Munich, Germany; [4]DZHK (Deutsches Zentrum für Herz-Kreislaufforschung [German Center for Cardiovascular Research]), Partner Site Munich Heart Alliance, Munich, Germany; and [5]Division of Nephrology, The Seventh Affiliated Hospital, Sun Yat-sen University, Shen Zhen, China